

JOURNAL OF THE ACADEMY OF CHEMISTRY TEACHERS

a biannual peer-reviewed research journal of chemistry

Vol : 2(2) • December 2016 • ISSN 2395-6801

Journal of the Academy of Chemistry Teachers (JACT) is a biannual peer reviewed journal published by the Academy of Chemistry Teachers, established in the year 1991. The journal is intended to promote innovative research in various novel fields of chemistry. The journal will cover all aspects of organic, inorganic and physical chemistry. Along with the frontier areas of chemistry like computational chemistry, combinatorial chemistry, green chemistry and nanochemistry, JACT aims to cover interdisciplinary areas such as chemistry education, chemistry of traditional medicines (ayurveda, siddha, homeopathy), biochemistry, cheminformatics, chemistry of materials, chemical technologies, chemistry of environment etc. **JACT** will publish review articles, short articles of popular interests and original research articles in any field of chemistry. **JACT** is intended to become a good journal for chemistry in its broadest sense.

Editor:

Dr. Reena Ravindran

Associate Professor of Chemistry,
Sree Narayana College,
Chempazhanthy, Thiruvananthapuram.
Email: reena1234@gmail.com
Mob: 9349321464

Editorial Board:

Dr. Sophia K. Philip

Associate Professor of Chemistry,
Christian College,
Chenganoor.
Email: sophia_kphilip@yahoo.com

Dr. R. Sudha Devi

Associate Professor of Chemistry
M.G College, Thiruvananthapuram.
Email: sudhamullor@gmail.com

Dr. Suma. S

Associate Professor of Chemistry,
Sree Narayana College,
Chempazhanthy, Thiruvananthapuram.
Email: sumasncw@gmail.com

Dr. Noeline B. Fernandez

Assistant Professor of Chemistry,
Fatima Mata National College, Kollam.
Email: fernandeznoeline@gmail.com

Dr. Radhika R. Nath

Assistant Professor of Chemistry,
DB College, Sasthamkottah, Kollam.
Email: rakhignath@yahoo.com

Advisory Committee:

Prof. George K. Thomas

Dean (Academic Affairs)
IISER, Thiruvananthapuram.

Dr. Mangalam S. Nair

Chief Scientist
CSIR-NIIST, Thiruvananthapuram.

Dr. K. N. Rajasekharan

Emeritus Professor
Department of Chemistry
University of Kerala, Kariavattom
Thiruvananthapuram.

Dr. Suresh Mathew

Professor & Director
School of Chemical Sciences
Mahatma Gandhi University
Kottayam.

Dr. M. R. Prathapachandra Kurup

Professor
Department of Applied Chemistry
Cochin University of Science & Technology
Kochi.

Prof. K. K. Aravindakshan

Professor (Retd),
Department of Chemistry
University of Calicut.

Dr. K. Anoop Krishnan

Scientist C
National Centre for Earth Science Studies
Akkulam, Thiruvananthapuram.

Dr. SMA Shibli

Professor & Head Department of Chemistry
University of Kerala.

Dr. T. S. Anirudhan

Professor
Department of Chemistry
University of Kerala.

JOURNAL OF THE ACADEMY OF CHEMISTRY TEACHERS

a biannual peer-reviewed research journal of chemistry

Vol : 2(2) • December 2016 • ISSN 2395-6801

CONTENTS

1. Kinetics Study of Plasticizer Migration from Commercial PVC Blood Storage Bag into Aqueous Organic Solvents 1-5
Sarath Josh M.K, Sudha Devi. R, Balachandran.S, Pradeep. S, Vijayalekshmy Amma. K.S
2. Bio-active Azo dyes from 3-(Pentadeca-8-enyl)phenol and Ortho Substituted Anilines 6-9
Jeena.V.R, Sreelatha .S.
3. Silane Modified Chitosan for Efficient Loading and Controlled Transdermal Release of Diltiazem 10-13
Anirudhan T S, Anoop S. Nair, Deepa J R
4. Investigation of the Morphology, Structure, Thermal and Electrical Property of Co/Ni Mixed Oxide Blended Polyaniline 14-20
Asha Bhanu A.V
5. A Comparative Study of the Ion Exchange Properties of Some Cerium (IV) Based Compounds 21-25
Apsara A. P, Beena B
6. Synthesis and Characterization of Tetraaquafumaratozinc(II): A 1D MOF with Supramolecular Assembly 26-32
Dhanya V.S, Sudarsanakumar M.R
7. A Glimpse to Thermal Decomposition Kinetics in Solid State 33-39
Jeena John, Sudha Devi R, Balachandran S

*Cover courtesy : Preparation of PEG coated VTMS-g-CS, Article 3, Page 10-13
Anirudhan T S, Anoop S. Nair, Deepa J R*

ACADEMY OF CHEMISTRY TEACHERS

Office Bearers

President

Dr. V. Sadasivan
University College, Thiruvananthapuram
sadasivan.v@gmail.com

Vice President

Dr. Reena Ravindran
SN College, Chempazhanthy
reena1234@gmail.com

General Secretary

Dr. Manohar D. Mullassery
FMN College, Kollam
mdmullassery@gmail.com

Treasurer

Dr. PK Reji
DB College, Sasthamcottah
pkreji@gmail.com

Dr. Sophia K. Philip
Christian College
Chenganoor

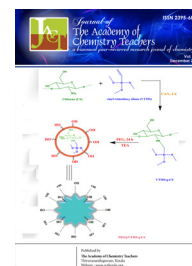
Secretary

Dr. TS Sujatha **Dr. K. V. Dinesh Babu**
MMNSS College Govt. College for Women
Kottiyam Thiruvananthapuram

Executive Committee Members

Dr. James T. Joseph, Mar Ivanios College, Tvpm
Prof. S. Shanavas, Govt. Arts College, Tvpm
Dr. Anoop MR, St. Stephen's College, Pathanapuram
Dr. Sreekumar PK, NSS College, Pandalam
Dr. Balachandran S. MG College, Tvpm

Dr. PG Chithra, SN College for Women, Kollam
Dr. KH Prema, SD College, Alappuzha
Dr. Abha K, Bishop Moore College, Mavelikkara
Dr. Rajasri Nair, MSM College, Kayamkulam
Dr. VL Siji, All Saint's College, Tvpm



Kinetics Study of Plasticizer Migration from Commercial PVC Blood Storage Bag into Aqueous Organic Solvents

Sarath Josh M.K.^{a,c}, Sudha Devi. R^b, Balachandran.S^{b*}, Pradeep. S^c, Vijayalekshmy Amma. K.S^a

^a Research & Post Graduate Department of Chemistry, Sri Vyasa N.S.S. College, Wadakkancherry, Thrissur, Kerala, India - 680 623

^b Department of Chemistry, Mahatma Gandhi College, Thiruvananthapuram, Kerala, India - 695 004

^c Enzyme Technology Laboratory, School of Biosciences, Department of Botany, University of Calicut, Kerala, India - 673 635

*Author for correspondence:

E-mail: sbcnair@gmail.com

Abstract

The leachability of di(2-ethylhexyl)phthalate (DEHP), a phthalate plasticizer known for their adverse health effects in test animals and in humans, from commercial polyvinyl chloride (PVC) blood bag into aqueous organic solvents such as acetonitrile:water and methanol:water were studied. The effect of temperature and solvent composition were also studied. The order of migration of DEHP during initial hours was acetonitrile:water > methanol:water. Fickian approximation was used to calculate the diffusion coefficient (D) for DEHP migration. Among the studied solvent systems, maximum D was observed ($1.57 \times 10^{-7} \text{cm}^2 \text{sec}^{-1}$ at 60 °C) in 90% acetonitrile:water, and the least ($1.36 \times 10^{-10} \text{cm}^2 \text{sec}^{-1}$) in 70% methanol:water at 25°C. Kinetic parameters of DEHP migration were calculated using Arrhenius rate equation; energy of diffusion was calculated and the maximum was observed for 70% methanol:water (63.68 kJ/g mol) and the least was observed in 90% acetonitrile: water compositions (28.71 kJ/g mol).

Keywords: Migration; Kinetics, PVC blood bag; Diffusion coefficient

Introduction

Phthalic acid esters or phthalates are ubiquitous environmental pollutants, known for their adverse health effects in test animals, and of late in humans, especially as endocrine disrupting chemical (EDC) [1, 2]. Employing *in silico* analyses, our group demonstrated the toxicity of phthalates and their metabolites [3, 4]. Among these toxic phthalates, di(2-ethylhexyl)phthalate (DEHP) is a widely used plastic softener in polyvinyl chloride (PVC) products such as blood and plasma bags, dialysis materials, tubing, toys, food packaging materials, building products, etc. [5-7]. PVC medical devices typically contain 10-40% DEHP by weight (singly or as a mixture of different phthalates including DEHP), and it can easily be leached out from the PVC matrix to the surroundings as it is not chemically bound to the PVC mesh [8, 9]. Migration of DEHP from PVC medical devices into the surrounding environments has been reported [10-12].

DEHP is poorly soluble in water, but dissolves efficiently in oil or fatty foods, and thus its highest concentrations have been detected in milk, cheese and fat deposits [13, 14]. DEHP is rapidly hydrolyzed into MEHP in human system and gets accumulated in tissues, blood cells and body fluids [15, 16], which in turn shown to cause hepatomegaly, reproductive and developmental toxicity, coupled with disruption of the endocrine system [17-

19]. Though the use of DEHP has partially or completely been banned in several countries, especially in toys, it is still the leading plasticizer being used in PVC-borne medical devices, because of its low cost and easy availability. David et al. [20] demonstrated that DEHP promoted the proliferation and hepatomegaly associated with hepatocellular tumorigenesis. Therefore, the European Union have banned the use of DEHP in toys, and restricted the daily intake upto 37 µg/kg. Migration of DEHP from the DEHP-PVC blood bag into the stored blood and blood components contained in it has much been studied. The release behavior of DEHP from flexible PVC is affected by the nature of surrounding medium, temperature, and the diffusion coefficient was directly proportional to the increasing temperature [8, 21]. Certain studies showed that treatment methods like UV-irradiation, mixing PVC with binary blends of phthalates, etc. are found to reduce the release of plasticizer from PVC materials [22, 23].

The objective of the present study was to determine the relationship between the release behavior of DEHP from PVC blood storage bags into two aqueous organic solvents such as acetonitrile:water and methanol:water systems by varying the quantity of both and to calculate the kinetic and thermodynamic parameters of DEHP migration.

Experimental

Reagents

Analytical grade DEHP was procured from VWR BDH Prolabo, India; AR grade acetonitrile and methanol were procured from Merck India P. Ltd. The commercial PVC blood storage bag (HL haemopak) was obtained from Hindustan Latex Ltd, Thiruvananthapuram, India (Batch No. HO 30419B, June 2013).

DEHP extraction method

The anti-coagulant solution contained in the whole blood bag (sample id HPB) was drained off, and washed thoroughly with double distilled water. PVC blood bag specimens were cut into small pieces of square size (7 mm²), and a weighed quantity (25 mg) of blood bag pieces was transferred into a refluxing apparatus containing 25 mL of *n*-hexane (*i.e.*, 1 mg/mL *n*-hexane) and refluxed for 3 h at 69 °C. The quantity of DEHP extracted into *n*-hexane from blood bag specimen was quantified using DEHP standard graph as described previously [8].

Migration study

For standard preparation, the optical density (OD) of known concentrations of DEHP in acetonitrile:water and methanol:water systems was measured using a UV-Vis spectrophotometer (Elico BL-200 Biospectrophotometer, India) at 275 nm. The migration behaviors of DEHP from blood bag into these solvent systems were studied at 25, 40, 50 and 60°C (in a thermo-stated water bath). One mg blood bag per mL each of these solvents was used for quantifying the migrated DEHP (in standard flask) in definite time intervals. Migration of DEHP was analyzed (OD at 275 nm) continuously at definite time intervals. Samples were withdrawn at every 5 min during the first 1 h, and then in every 30 min interval. Immediately after OD measurement, the sample poured back in the migration system so that the total volume was kept constant. The weight of migrated DEHP in solvents was calculated by fitting the values on to the standard graph as previously reported [8].

Statistics

One dimensional Fick's law may describe the leaching, transferring and diffusion phenomena of relatively small molecules through flexible polymers, and it is represented by

$$M_t / M_{\infty} = 2 (Dt/\pi l^2)^{1/2}$$

Where, M_t represents the DEHP released at time t and M_{∞} is the total DEHP originally present in the specimen (blood bag), D is the diffusion coefficient (D) and l denotes the thickness of the specimen.

Percentage of phthalate migration was calculated using the formula,

$$\% = (C_t / C_i) \times 100$$

Where C_i is the total phthalate contained in the blood bag, and C_t is the quantity of phthalate migrated in to the surrounding solvent in time t . Thermodynamic calculations were done using the relations as given below.

Energy of migration can be calculated using Arrhenius equation,

$$D = D_0 e^{-E_D / RT}$$

Where D is the diffusion coefficient, D_0 is the diffusion coefficient at standard temperature (25 °C), R is the universal gas constant (8.314 JK⁻¹mol⁻¹) and E_D is the energy of diffusion. The data presented here are average values of at least three independent values with \pm SD. Microsoft Excel was used to plot the graph.

Results and discussion

Migration pattern of DEHP

After extraction with *n*-hexane, it was found that the commercial blood bag used for this study contained 35.48 \pm 0.30% DEHP by weight. **Figure 1A-D** depicts the release behavior of DEHP from HPB blood bag into three different aqueous compositions of acetonitrile at 25, 40, 50 and 60 °C. Of the three aqueous compositions, 90% acetonitrile emerged as good solvent for faster migration of DEHP. A total of 25.13, 31.10 and 37.45% of DEHP were found to be migrated into 70, 80 and 90%, respectively at 25 °C for 1 h (**Figure 1A**). Compared to the weight of PVC blood bag, 8.99, 11.14 and 13.40% weight loss were observed in 70, 80 and 90%, respectively at 25 °C for 1h. DEHP migration rate at 40 °C (**Figure 1B**) and 50 °C (**Figure 1C**) was in between 25 and 60 °C. **Figure 1D** depicts the migration of DEHP in acetonitrile:water at 60 °C for 1h. Maximum DEHP migration was observed at 60 °C, *i.e.*, 50.91, 62.79 and 68.08% DEHP were found to be migrated into 70, 80 and 90% acetonitrile, respectively. At this temperature, total weight loss of blood bag was 18.22, 22.48 and 24.37 at 70, 80 and 90% acetonitrile, respectively for 1h. It is very clear that DEHP migration increases upon increasing the temperature of the surrounding medium (**Figure 1A-D**).

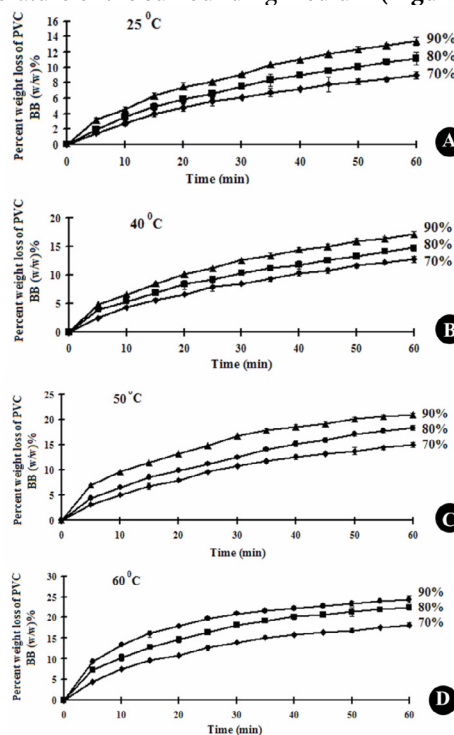


Figure 1. Migration behavior of DEHP in acetonitrile:water at different temperatures; (A), at 25°C, (B), at 40°C, (C), at 50°C and, (D), at 60°C.

The release behaviors of DEHP from HPB PVC blood bag into methanol:water systems at 25, 40, 50 and 60°C for 6h were investigated (Figure 2A-D). During the analysis, at 25 °C (for 6 h), PVC blood bag showed a weight loss of 2.24, 3.52 and 4.54%, respectively in 70, 80 and 90% methanol (Figure 2A). Migration rates at 40 (Figure 2B) and 50 °C (Figure 2C) were in between 25 and 60 °C. At 60 °C (for 6 h), 6.57, 11.44 and 13.42% weight loss were observed in blood bag in 70, 80 and 90% methanol, respectively (Figure 2D). When the release behavior of DEHP from PVC blood bag into these two aqueous organic solvents was compared, acetonitrile:water was emerged as a good solvent system for the faster migration analysis. It is evident that, DEHP migration increases upon increasing the temperature of the methanol:water system (Figure 2A-D). Gotardo and Monteiro, [24] reported the migration of DEHP from PVC bags into intravenous cyclosporine solutions. Transport phenomena of DOP into and out of plasticized PVC sheets in alcohols were studied [25]. Migration of plasticizers from PVC gaskets of lids for glass jars into oily foods [26], aqueous solvents [21], organic solvents [8] were reported. Plasticizer transfer from plasticized PVC sheets into petroleum oils have been explained and aspects of D have been reported [27]. Marcilla et al. [28] introduced a method for the study of migration of the plasticizer from a plasticized PVC, when it comes in contact with unplasticized polymer.

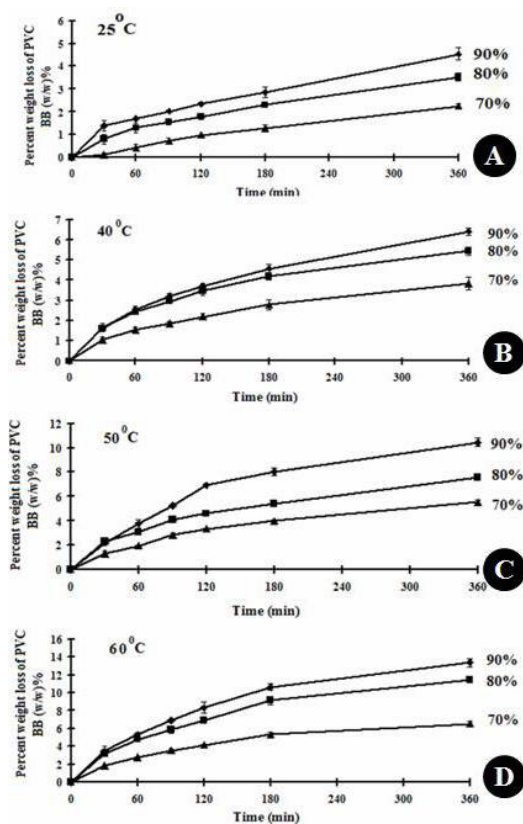


Figure 2. Migration behavior of DEHP in methanol:water at different temperatures; (A), at 25°C, (B), at 40°C, (C), at 50°C and, (D), at 60°C.

Diffusion coefficient (D)

Fick's law of diffusion was applied for the calculation of the diffusion coefficient (D). Assume that PVC films are perfectly planar and DEHP primarily diffuses through the surface of the film (*i.e.*, release of DEHP through the edge of the film is negligible), and the volume of leaching solvent is very large, compared to the amount of released DEHP, good linear functional relation between M_t/M_∞ and $t^{1/2}$ at various compositions (90, 80 and 70%), and at different temperatures (25, 40, 50 & 60 °C) were obtained. The D calculated from the modulus of the straight line is listed in Table 1. The present data depict that D was directly proportional to the temperature of the surrounding medium and the percentage of the organic solvent (Figures 3). D is maximum in 90% acetonitrile:water, which is $1.57 \times 10^{-7} \text{cm}^2 \text{sec}^{-1}$ at 60 °C. In 70% methanol:water at 25°C, D was $1.36 \times 10^{-10} \text{cm}^2 \text{sec}^{-1}$ (Table 1). At 30 and 40 °C, DEHP migration and D were calculated for 30/70, 40/60 DEHP/PVC plasticized PVC sheets into acetonitrile and ethanol:water mixtures, and D was in between $2.72\text{-}10.1 \times 10^{-10} \text{cm}^2 \text{sec}^{-1}$ [21]. Similarly, D was calculated for PVC tubing used for intravenous administration, and PVC membrane at 5 and 40 °C were 9.1 and $156 \times 10^{-10} \text{cm}^2 \text{min}^{-1}$ in aqueous Tween 80 solutions [11]. According to the previous reports, D depends on the nature of surrounding medium, temperature of the surrounding medium [11, 29], the molecular weight of the plasticizers used [28], decrease with increase in alkyl group length, decrease with increase in alkyl group branching [30], and circulation speed of the circulating fluids through the PVC tubings [11].

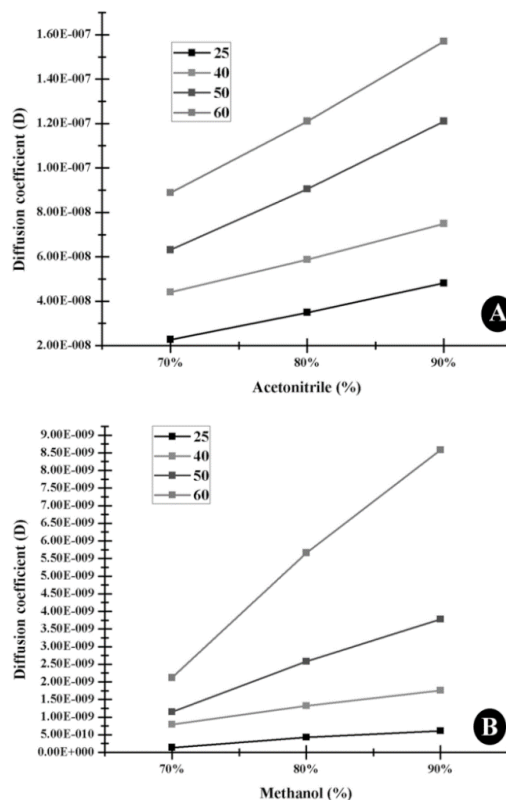


Figure 3. Linearity of the diffusion coefficient (D) with the varying percentage of; (A). Acetonitrile:water. (B). Methanol:water at different temperatures.

Thermodynamics of DEHP migration

By considering, D_0 as the diffusion coefficient at standard temperature (25 °C), activation energy (E_D) and drawing the curve of $\ln(D/D_0)$ with inverse temperature ($1/T$). The E_D could be calculated from the slope of the linear graph ($-E_D/R$) [30, 31]. At 70% acetonitrile:water mixture, the E_D was 32.16, and 63.68 kJ/mol was for 70% methanol:water system (Table 2); while 28.71 for 90% acetonitrile:water, and in 90% methanol:water 61.16 kJ/mol were observed. It is evident that E_D is decreasing upon increasing the percentage of polar organic solvents. As the percentage of organic component increases the percentage solubility increases, there by the diffusion probability increases. The nature of the matrix, temperature of the solvent, time of contact with the solvent/medium etc, influence the nature of migration of plasticizers from PVC matrix. A very low value of E_D (310.37 J/g mol) were reported for the migration of DEHP from PET bottles into yogurt

drinks[31], however 22.0 and 7.9 kcal/mol were observed for di-n-hexyl phthalate diffusion above and below the PVC glass transitions, respectively [30]. E_D values found within 70–108 kJ/mol at higher temperatures (120–150 °C) for the phthalate plasticizers in plasticized PVC [32], 93.2 kJ/mol for DEHP [33]. In our previous study, the temperature and solvent dependent migrations of DEHP from commercial PVC blood storage bags and diffusion coefficients were calculated using one dimensional Fick's law and short time Fickian approximation during the release of DEHP [8]. It suggests that upon rise in temperature, the PVC matrix gets loosened, facilitating faster liberation of the physically bound DEHP from the PVC mesh. In this study, the DEHP migration kinetics was in good conformity to the short time Fickian approximation, as proposed by Duvis et al. [34].

Table 1. Diffusion coefficient (D) of DEHP calculated using Fick's first law of diffusion in the aqueous mixtures of acetonitrile and methanol.

Temp (°C)	Diffusion coefficient, D (cm ² sec ⁻¹)					
	70%		80%		90%	
	acetonitrile	methanol	acetonitrile	methanol	acetonitrile	methanol
25	2.27×10 ⁻⁸	1.36×10 ⁻¹⁰	3.49×10 ⁻⁸	4.28×10 ⁻¹⁰	4.81×10 ⁻⁸	6.13×10 ⁻¹⁰
40	4.41×10 ⁻⁸	7.94×10 ⁻¹⁰	5.87×10 ⁻⁸	1.32×10 ⁻⁹	7.49 ×10 ⁻⁸	1.76×10 ⁻⁹
50	6.31×10 ⁻⁸	1.15×10 ⁻⁹	9.05×10 ⁻⁸	2.58×10 ⁻⁹	1.21×10 ⁻⁷	3.78×10 ⁻⁹
60	8.88 ×10 ⁻⁸	2.12×10 ⁻⁹	1.21×10 ⁻⁷	5.86×10 ⁻⁹	1.57×10 ⁻⁷	8.58×10 ⁻⁹

Table 2. Energy of diffusion calculated for DEHP migration from HPB into aqueous mixtures for various compositions.

Solvent (%)	Energy of diffusion, E_D (KJ/g mol)	
	Acetonitrile:water	Methanol:water
70	32.16	63.68
80	29.82	60.95
90	28.71	61.16

Conclusions

When effects of two aqueous organic solvents such as acetonitrile:water, methanol:water on the rate of migration of intact DEHP from blood bag were tested at various temperatures and compositions of water, the order of migration of DEHP during initial hours was acetonitrile:water > methanol:water. The D was the maximum in 90% acetonitrile:water (1.57×10⁻⁷ cm² sec⁻¹) at 60 °C, and the least (1.36×10⁻¹⁰ cm² sec⁻¹) was found in 70% methanol:water at 25 °C. Comparison of

D in acetonitrile:water and methanol:water at different temperatures and at various aqueous compositions showed that the diffusion process was temperature dependent, in tune with the Fickian approximation and Arrhenius relation.

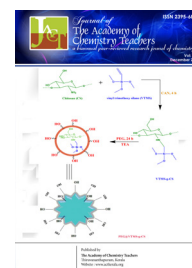
Acknowledgements

The authors would like to thank the Ministry of Environment and Forests, Government of India for a research Grant No. 19/62/2005-RE. The authors declare that there exists no conflict of interest.

References

- Hauser R & Calafat A, *Occup Environ Med*; 62 **2005**, 806-818.
- Benson R, *Regul Toxicol Pharm*; 53 **2009**, 90-101.
- Sarath Josh MK, Pradeep S, Adarsh VK, Vijayalekshmi Amma KS, Sudha Devi R, Balachandran S, Sreejith MN, Abdul Jaleel UC & Benjamin S, *Mol Simul*; 40 **2014a**, 408-417.
- Sarath Josh MK, Pradeep S, Vijayalekshmi Amma KS, Balachandran S, Abdul Jaleel UC, Doble M, Spener F & Benjamin S, *J Appl Toxicol*; 34 **2014b**, 754–765.

5. David RM, McKee RH, Butala JH, Barter RA & Kayser M, In: Patty's Industrial Hygiene and Toxicology, Vol. 6, Wiley, New York, **2001**, pp. 635-932.
6. Jenke D, PDA J Pharm Sci Tech; 60 **2006**,191-207.
7. Tümay Özer E & Güçer Ş, Polym Test; 31 **2012**, 474-480.
8. Sarath Josh MK, Pradeep S, Balachandran S, Sudha Devi R, Vijayalakshmi Amma KS & Benjamin S, J Polym Res; 19 **2012**, doi:10.1007/s10965-012-9915-4.
9. Wildbrett G, Environ Health Perspect; 3 **1973**, 29-35.
10. Haishima Y, Seshimo F, Higuchi T, Yamazaki H, Hasegawa C, Izumi S-i, Makino T, Nakahashi K, Ito R, Inoue K, Yoshimura Y, Saito K, Yagami T, Tsuchiya T & Nakazawa H, Int J Pharm; 298 **2005**,126-142.
11. Hanawa T, Naoko E, Masahiko S, Katsuhide T, Moriyuki O, Keizoh S, Mutsuko T, Kenji K, Shin'ichiro N & Toshio O. Int J Pharm; 297 **2005**, 30-37.
12. Hanawa T, Muramatsu E, Asakawa K, Suzuki M, Tanaka M, Kawano K, Seki T, Juni K & Nakajima Si, Int J Pharm; 210 **2000**, 109-115.
13. Sørensen LK, Rapid Commun Mass Sp; 20 **2006**, 1135-1143.
14. Sharman M, Read WA, Castle L & Gilbert J, Food Addit Contam; 11 **1994**, 375-385.
15. Thomas JA, Curto KA & Thomas MJ, Environ Health Perspect; 45 **1982**, 85-88.
16. Takatori S, Okamoto Y, Kitagawa Y, Hori S, Izumi S-I, Makino T & Nakazawa H, Int J Pharm; 352 **2008**, 139-145.
17. Kluwe WM, Environ Health Perspect; 65 **1986**, 271-278.
18. Huber WW, Grasl-Kraupp B & Schulte-Hermann R, CRC Crit Rev Toxicol; 26 **1996**, 365-481.
19. Turnbull D & Rodricks JV, Int J Toxicol; 4 **1985**, 111-145.
20. David RM, Moore MR, Cifone MA, Finney DC & Guest D, Toxicol Sci; 50 **1999**, 195-205.
21. Kim JH, Kim SH, Lee CH, Nah JW & Hahn A, Bull Kor Chem Soc; 24 **2003**, 345-349.
22. Thomas N, J Appl Polym Sci; 94 **2004**, 2022-2031.
23. Lakshmi S & Jayakrishnan A, Polymer; 39 **1998**, 151-157.
24. Gotardo M & Monteiro M, J Pharm Biomed Anal; 38 **2005**, 709-713.
25. Papaspyrides CD, J Appl Polym Sci; 32 **1986**, 6025-6032.
26. Fankhauser-Noti A & Grob K, Trends Food Sci Tech; 17 **2006**, 105-112.
27. Papaspyrides CD & Duvis T, J Appl Polym Sci; 38 **1989**, 1573-1580.
28. Marcilla A, García S & Garcia-Quesada J, Polym Test; 27 **2008**, 221-233.
29. Papaspyrides CD & Duvis T, Polymer; 31 **1990**, 1085-1091.
30. Storey RF, Mauritz KA & Cox BD Macromol; 22 **1989**, 289-294.
31. Farhoodi M, Emam-Djomeh Z, Ehsani MR & Oromiehie A, Arabian J Sci Eng; 33 **2008**, 279-287.
32. Kovačić T & Mrklić Ž, Thermochim Acta; 381 **2002**, 49-60.
33. Ekelund M, Edin H & Gedde UW, Polym Degrad Stab; 92 **2007**, 617-629.
34. Duvis T, Karles G & Papaspyrides CD, J Appl Polym Sci; 42 **1991**, 191-198.



Bio-active Azo dyes from 3-(Pentadeca-8-enyl)phenol and Ortho Substituted Anilines

Jeena.V.R *, Sreelatha .S.

Department of chemistry, N S S College, Pandalam, Pathanamthitta, Kerala, India - 689501

*Author for correspondence:

E-mail: jeenalaljith@gmail.com

Abstract

Two new azo dyes synthesized from a natural renewable source, 3-(pentadeca-8-enyl)phenol and ortho substituted anilines, *o*-aminophenol and *o*-toluidine were characterized using UV-Visible and FTIR spectroscopy. The compounds were evaluated for their antibacterial activity against *Staphylococcus aureus* and *Escherichia coli* by disc diffusion method. The screening data revealed that the dyes exhibited potent antibacterial activity against both bacterial strains.

Keywords: azo dyes, 3-(pentadeca-8-enyl) phenol, *o*-aminophenol, *o*-toluidine, antibacterial

1. Introduction

Azo dyes are majorly used in textile industry, besides their applications in fields like cosmetics, food industry, medicines, plastics, automobile industry etc¹⁻⁴. Azo dyes were reported to have been synthesised with the coupling reactions 3-(pentadeca-8-enyl)phenol, a meta substituted unsaturated phenol obtained from cashew nut shell liquid a natural renewable source, with the diazotized aniline, *m*-toluidine⁵, *p*-anisidine and *p*-sulphanilic acid⁶. Antibacterial activity of azo dyes is also well-known⁷. The dyes synthesized from *p*-anisidine and *p*-sulphanilic acid exhibited potent antibacterial activity against *B. cereus* and *K. pneumonia*⁶.

In the present study *o*-aminophenol and *o*-toluidine are diazotized separately and then coupled with 3-(pentadeca-8-enyl) phenol (figure 1) to produce diazotized *o*-aminophenol 3-(pentadeca-8-enyl) phenol dye and diazotized- *o*-toluidine 3-(pentadeca-8-enyl) phenol dye respectively. They are characterized by UV and FT-IR spectroscopic techniques and their antibacterial activity has also been studied.

2. Materials and Method

3-(Pentadeca-8-enyl) phenol was obtained from M/s Golden Cashew Chemicals Ltd, Mangalore. Sodium nitrite, potassium hydroxide, *o*-aminophenol, *o*-toluidine and methanol were received from Loba Chemie. The chemicals were used as received. Ultraviolet spectral analysis was carried out in a SCHIMADZU 1800 UV Spectrophotometer. Infrared spectra were taken in a PERKIN-ELMER Spectrum 400 IR spectrophotometer by KBr pellet method.

2.1 Synthesis of the Dyes

The procedure adopted for the synthesis of dyes was as reported earlier⁸. orthoaminophenol (3g - 27.5 μmol)

was dissolved in 25 mL of 1:1 Hydrochloric acid. A solution of sodium nitrite (0.92g - 13.3 μmol) in distilled water (3mL) was prepared and added drop wise to the acidic solution of amine over a period of 10 min and the mixture was stirred at 0 °C for 50 min. The pH of diazonium solution of amines was adjusted to 8 by the addition of appropriate amount sodium bicarbonate (1M) solution. The pre-cooled solution of 3-(pentadeca-8-enyl) phenol (3.2g - 10.7 μmol) in 15 mL ethanol was injected drop wise to the above pH monitored solution at 0 °C. The reaction mixture was stirred at 0 °C for 40 min by which time the product was precipitated. The water insoluble portion was extracted with diethyl ether, the organic layer was washed repeatedly with 50 mL distilled water and solvent was removed under reduced pressure. Resulting dye was dried in vacuum oven. A portion of the dye was recrystallised from hexane –chloroform (8:2) mixture.

Similarly *o*-toluidine-3-(pentadeca-8-enyl) phenol azo dye was synthesised following the same procedure as given above by taking *o*-toluidine (3g - 28.04 μmol). The dye obtained as reddish brown viscous liquid was purified by column chromatography.

2.2 Antibacterial Studies

Antibacterial activities of the synthesised dyes were carried out against Gram-positive (*Staphylococcus aureus*) and Gram-negative (*Escherichia coli*) bacterial strains using disc diffusion method. Finally their activities were compared. Nutrient agar was used as the medium for the preparation of pure cultures of bacteria for detecting antibacterial activity. Test organisms were collected from Institute of Microbial Technology, microbial type culture collection centre, (IMTECH), Chandigarh.

The bacterial strains were maintained on their respective medium in slants at 2-8 °C. Muller Hinton Agar (MHA) medium was used for bacterial culture. MHA was prepared and sterilized at 121 °C for 15 min. After sterilization required volume of the medium (20 mL) was poured in the sterile petridishes and allowed to solidify. Sensitivity of the 0.1 g dye were tested for both Gram-positive (*Staphylococcus aureus*) and Gram-negative (*Escherichia coli*) bacterial strains that are resistant to a broad band of antibiotics excluding ampicillin. Dimethyl

sulfoxide (DMS) was used as the negative control to compare the antibacterial activity in all experiments.

3. Results and Discussion

The dye 1 formed by the diazotization of *o*-aminophenol with 3-(pentadeca-8-enyl)phenol was obtained as reddish brown crystals and dye 2 formed by the diazotisation of *o*-toluidine with 3-(pentadeca-8-enyl)phenol was obtained as reddish brown viscous liquid. They were soluble in methanol, ethanol, acetone, hexane and toluene.

The scheme of synthesis of the dyes is as shown where R= OH for Dye 1 and CH₃ for dye 2.

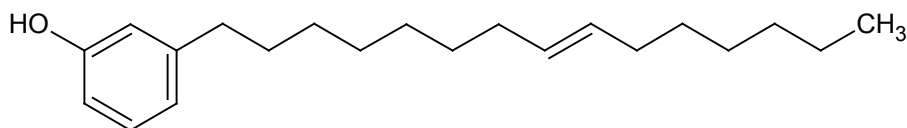
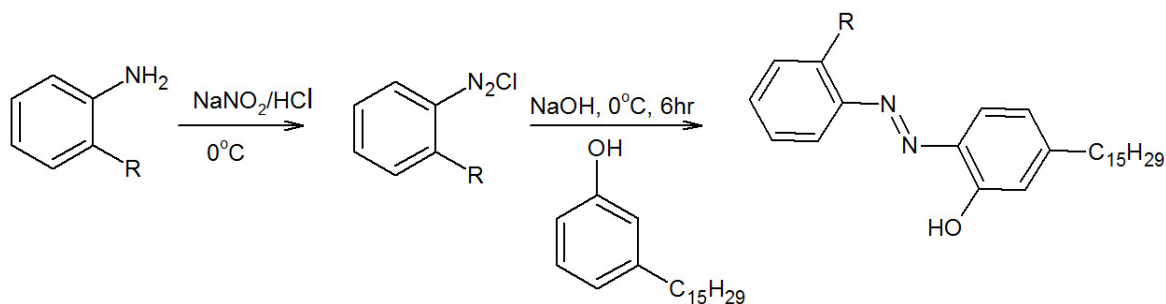


Figure 1: Structure of 3-pentadeca-8-enylphenol obtained from cashew nut shell



Scheme 1: Synthesis of azo dyes

The syntheses of dyes were depicted in scheme 1. The UV spectrum in the range 250 nm to 700 nm were presented in figure 2. The UV spectrum of *o*-aminophenol-3-(pentadeca-8-enyl) phenol dye shows sharp peak at 378 nm, which is related to the $n-\pi^*$ transition of azo unit of the dye and a sharp peak at 267 nm which is attributed to aromatic phenyl ring. The corresponding peaks in *o*-toluidine dye were obtained at 360 nm and 283 nm.

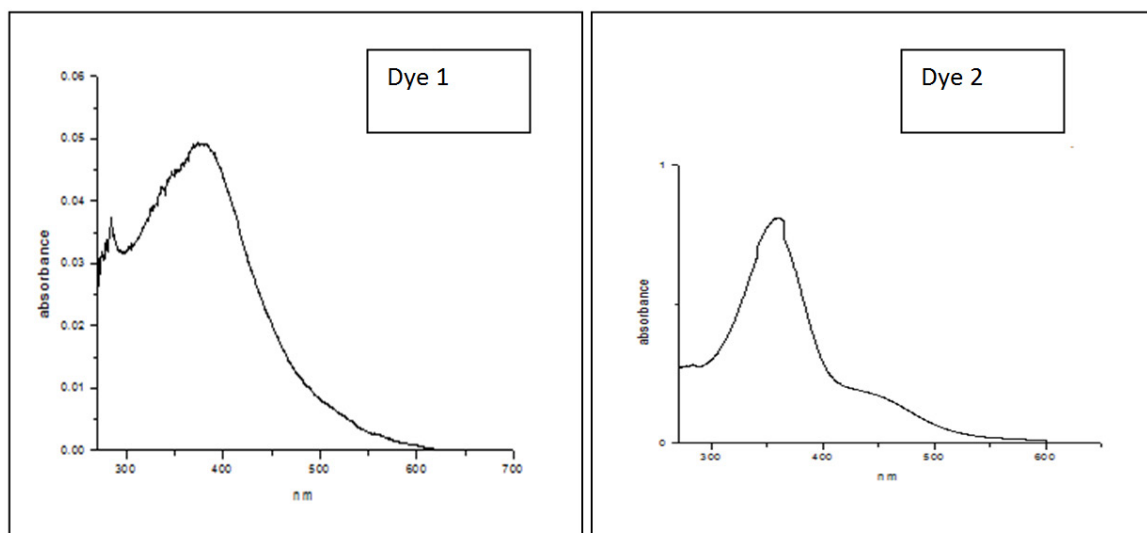


Figure 2: UV spectrum of the dyes

In the FTIR spectrum of *o*-aminophenol dye, The peaks such as 3500 – 3300 cm^{-1} (O – H hydrogen bonded), 2924 and 2847 cm^{-1} (symmetric C – H stretching), 1635 cm^{-1} (C=C stretching of aromatic ring) and a peak at 1458 cm^{-1} is due to –N=N– stretching of azo group.

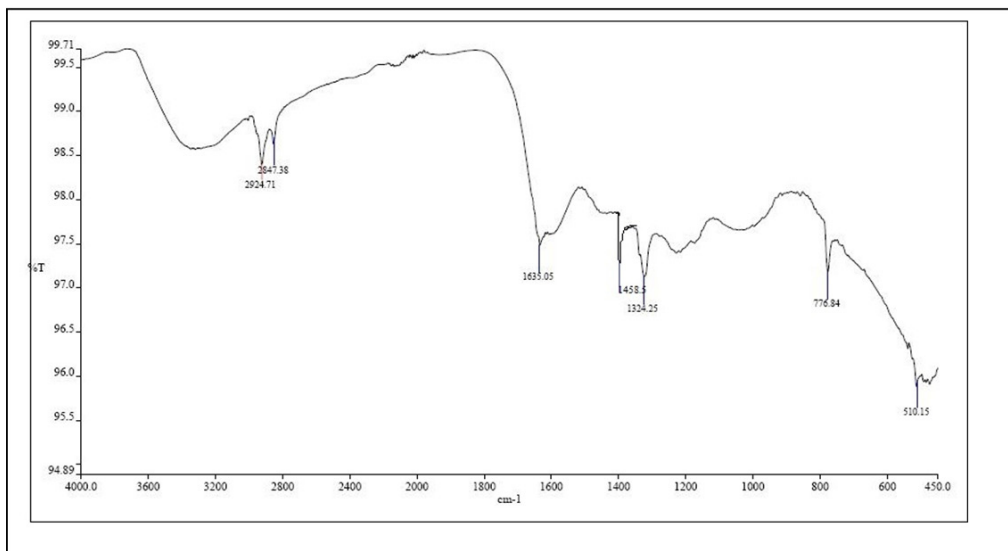


Figure 3: IR spectra of o-aminophenol Dye

The IR spectrum of o-toluidine-3-(pentadeca-8-enyl) phenol dye (figure 3) shows broad peak in the region 3500 – 3300 cm^{-1} (O – H hydrogen bonded), 2921, 2851 cm^{-1} (symmetric C – H stretching), 1595 cm^{-1} (C= C stretching of aromatic ring), 1250 cm^{-1} (C-O stretching in COOH group) and a peak at 1463 cm^{-1} due to –N=N–stretching of azo group.

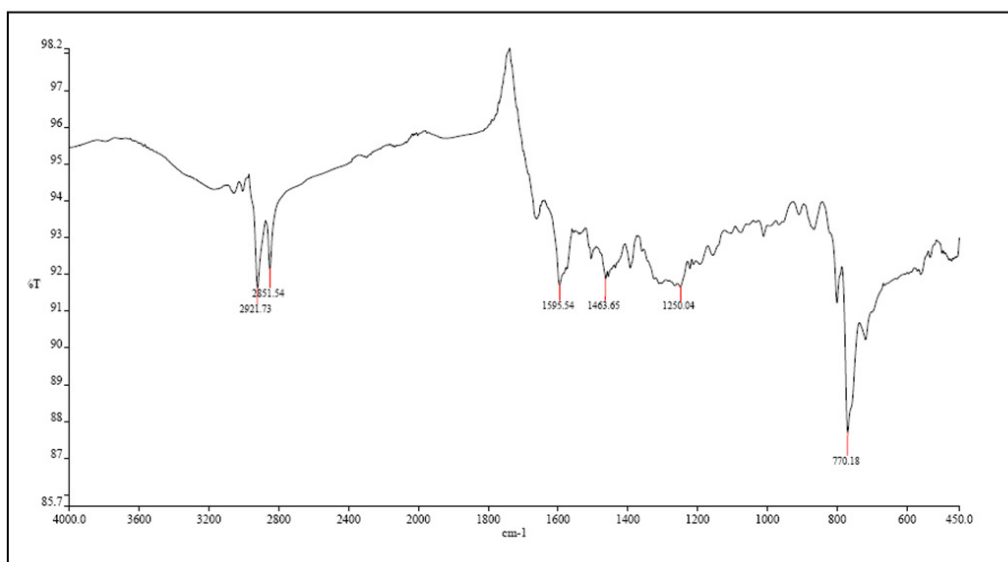


Figure 4: IR spectra of o-toluidine Dye

3.1 Antibacterial Studies

Table 1 shows the antibacterial activities of the dyes against *Staphylococcus aureus* and *Escherichia coli* respectively. The results indicate that both the dyes show good antibacterial activity against gram negative *E. coli* and

gram positive *S. aureus*. Figure 12 shows the inhibition zones. (C denotes control, 1551 and 1554 denotes o-aminophenol and o-toluidine dyes respectively).

Sample	Organism	Zone of inhibition (mm) Diameter
o-aminophenol dye	<i>S. aureus</i>	10
	<i>E. coli</i>	7
o-toluidine dye	<i>S. aureus</i>	12
	<i>E. coli</i>	7
Control	<i>S. aureus</i>	0
	<i>E. coli</i>	0

Table 1: Antibacterial activities of dyes

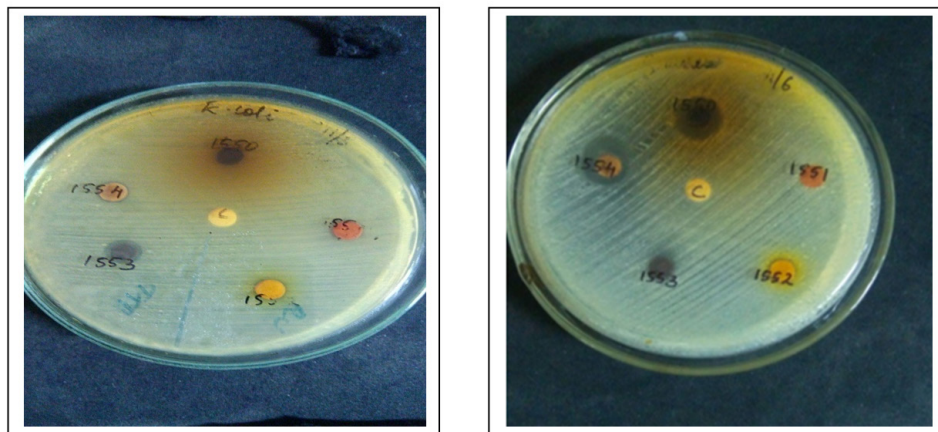


Figure 5: Zones of inhibition of dyes

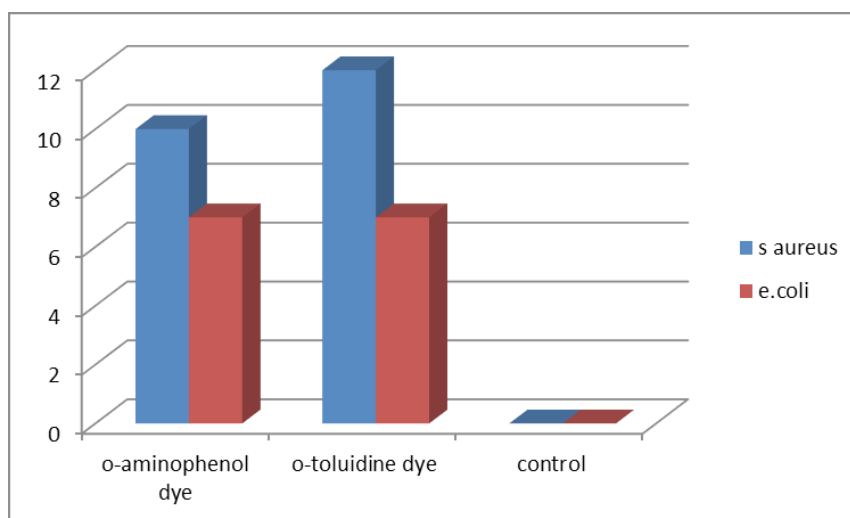


Figure 6: Proportion Index of antibacterial activity of the dyes

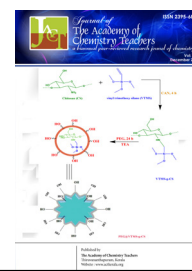
4. Conclusion

Two bio based azo dyes were prepared by the diazotization of *o*-aminophenol, *o*-toluidine and coupling with 3-(pentadeca-8-enyl) phenol to produce diazotized *o*-aminophenol 3-(pentadeca-8-enyl) phenol dye and *o*-toluidine 3-(pentadeca-8-enyl) phenol dye respectively. They have been characterized by UV and FT- IR spectroscopic techniques and their antibacterial

properties were studied. Antibacterial activity experiments performed on the two microorganisms clearly demonstrated the higher effectiveness of these dyes against both Gram negative bacteria and Gram positive bacteria. Hence these dyes can be used to discover bioactive natural products that may serve as leads in the development of new pharmaceuticals.

References

- Mittal A, Kurup L & Mittal J, J Haz, Mat, 146, **2007**, 243.
- JSimu G, Chicu S A, Morin N, Schmidt W & Sisu E, Turk J Chem, 28, **2004**, 579.
- Bae J S, Freeman H S & El-Shafei A, Dyes and Pigments, 57, **2003**, 121.
- Combellas C, Kanoufi F, Pinson H & Podyorica F, Am Chem Soc, 34, **2008**, 429.
- Das T K, Int J Appl Sci Biotechnol, 2(2), **2014**, 176-179.
- Gopalakrishnan S, Nevaditha N T & Mythili C V, J Chem Pharm Res, 3(4), **2011**, 490-497.
- Harisha S1, Keshavayya J, Patil S R & Maliyappa M R, Asian J Biochem Pharm Res 5, **2015**, 82-100.
- Maqbool H, Ganesh S D & Pai V K, Der Pharma Chemica, 5(5), **2013**, 154-159.



Silane Modified Chitosan for Efficient Loading and Controlled Transdermal Release of Diltiazem

Anirudhan T S*, Anoop S. Nair, Deepa J R

Department of Chemistry, School of Physical and Mathematical Sciences, University of Kerala, Kariavattom, Trivandrum, Kerala, India - 695 581

*Author for correspondence:

E-mail: tsani@rediffmail.com

Abstract

Due to stressful modern life, cases of cardiac failures are continuously increasing. Transdermal drug delivery systems (TDDS) serve as efficient administration route, as they can overcome conventional administration's demerits. However, efficient calcium channel blockers like diltiazem (DTZ) are highly hydrophilic and require vehicles that simultaneously possess hydrophilicity with some hydrophobicity. Herein, we report a novel TDDS of poly ethylene glycol coated vinyl trimethoxy silane-g-chitosan (PEG@VTMS-g-CS) possessing hydrophilicity to ensure efficient DTZ encapsulation as well as hydrophobicity to facilitate skin penetration. Well characterized TDDS using IR, XRD and SEM also exhibited sustained release with minimal swelling of the matrix.

Keywords: Transdermal drug delivery, diltiazem, PEG, silane modified chitosan, controlled release.

1. Introduction

Due to the stress and strain offered by the modern day life, the number of hypertensive patients has gone up tremendously. According to World Health Organization, 7.5 million deaths occur around the globe due to hypertension every year. Modern science has discovered many efficient drugs like amlodipine, diltiazem hydrochloride (DTZ), verapamil, etc. Even then, various factors like hepatic first pass metabolism, frequent dosing, etc. have limited their clinical use as an oral drug. In fact, due to the extensive first pass metabolism, bioavailability of DTZ falls to a drastic 30.0 - 40.0 % when administered orally. All these drawbacks call for alternate route for DTZ administration.

Drug delivery through skin, termed as TDDS, can overcome all the drawbacks of conventional drug administration and also possess advantages like patient compliance, sustained release as well as non-requirement of a trained personnel. DTZ is an efficient calcium channel antagonist which belongs to the class of benzothiazepines that are commonly used in the treatment of angina pectoris, hypertension and some types of arrhythmia [1]. Even though there are many reports for DTZ transdermal delivery, owing to the differences in miscibility, better results are seldom observed.

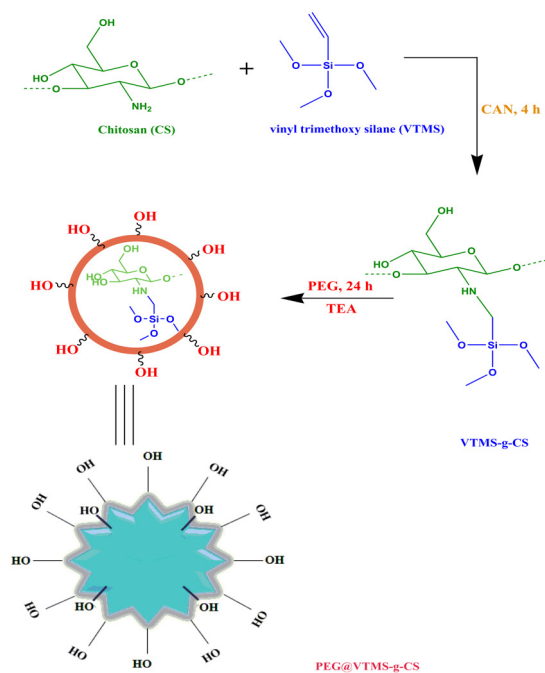
Due to the hydrophilicity of DTZ, it requires a hydrophilic drug carrier for efficient drug encapsulation. On the other hand, due to lipophilicity of the skin, drugs are not well permeated unless their vehicles are hydrophobic. This discrepancy makes the transdermal delivery of DTZ a big challenge. Herein, we report a novel strategy to achieve efficient encapsulation and sustained

transdermal release of DTZ. In the present approach, a copolymer: poly ethylene glycol coated vinyl trimethoxy silane - grafted- chitosan was developed and dispersed in various biodegradable matrices like alginic acid (ALG), carboxy methyl cellulose (CMC) and poly vinyl alcohol (PVA). The selection of these matrices was based on their biocompatibility, biodegradability, mechanical strength of films, ease of preparation and hydrophilicity. Further, the dispersion strategy was useful as it increased the permeation pathway thereby delaying the drug release. The prepared material was characterized using FTIR, XRD and SEM techniques. Swelling of the matrix at acidic and basic pH, *in vitro* permeation studies on rat skin and its histological analysis were performed to evaluate the practical utility of the prepared material in real life situations.

2. Materials and Methods

2.1 Preparation of DTZ loaded PEG@VTMS-g-CS: 15 mL VTMS was initiated with 10 mL benzoyl peroxide. This was added to a previously initiated CS solution, prepared by adding 10 mL (v/v) 0.1 M CAN to 100 mL 2.0 % CS solution. The mixture was heated to 40 °C with constant stirring for 3 - 4 h. The product was then precipitated in excess 10.0 % NaOH with vigorous stirring. The graft product was then washed with water for removing homopolymers. For coating the copolymer with PEG, 0.1 g of the synthesized VTMS-g-CS was dissolved in about 20 mL (v/v) methanol. This solution was added to a mixture of 1 mL (v/v) PEG and 0.5 mL (w/v) TEA. The solution was stirred for about 3-4 h. The

white precipitate thus obtained was centrifuged, washed with water and dried. The schematic representation of the DDS is as shown in Scheme 1. DTZ was loaded onto the hydrophilic core created by the copolymer using hydrogen bonding interactions. Briefly, 0.07 g (w/v) PEG@VTMS-g-CS was dissolved in 20 mL methanol. To this solution, 0.035 g (w/v) of DTZ in 20 mL water was added drop wise with continuous shaking for about 4 h. The product was then centrifuged, washed with water and dried.



Scheme 1. Preparation of PEG coated VTMS-g-CS

2.3 Determination of swelling degree %: To verify whether the prepared copolymer swells, its SD % was determined at pH 1.2 and 7.4. Swelling measurements were performed by immersing the DDS taken in tea bag in respective buffer solutions. The weight of swollen copolymer was measured at different time intervals after removing the surface water with filter paper. Degree of swelling was calculated using equation 1 as:

$$\text{Degree of swelling \%} = \frac{(W_s - W_i)}{W_d} \times 100 \quad (1)$$

where, 'w_s' is the weight of the swollen copolymer at a given time during swelling, 'w_i' is the initial weight, 'w_d' is the weight of the dry copolymer.

2.4 In vitro release profile: The sustained drug release action of the TDDS was evaluated using a previous procedure reported by our group on wistar rats using modified Franz diffusion cell [2]. Briefly, male wistar rats were euthanized with prolonged chloroform inhalation. Abdominal hairs were removed using hair trimmer. *In vitro* skin permeation was conducted using modified glass Franz diffusion cell with a permeation area of 0.95 cm² and with a receptor volume of 4 ml. The thermally isolated epidermis including stratum corneum was mounted between donor and receptor chambers of the diffusion cell with the stratum corneum facing the donor

compartment and the other side in direct contact with the receptor medium. The tissue was then kept in intimate contact by tightly wrapping parafilm at the junction. Receiving chamber was filled with PBS (pH = 7.4) and was thermostated to 37 °C. Each drug loaded patches was placed in intact epidermal membrane of the donor compartment and was wetted with PBS. The receptor fluid was constantly mixed using magnetic stirrer at 750 rpm. Aliquots from the stirred receptor compartment were withdrawn using a glass syringe at definite time intervals, and was replaced with same volume of the pre warmed physiological saline to maintain the sink condition.

3. Results and Discussion

3.1. Characterisation of the TDDS: The FTIR spectra of all the samples are as shown in Fig. 1. Spectrum of CS showed characteristic broad peak around 3315 cm⁻¹ due to the overlapping of O-H and N-H stretching. VTMS showed absorption peak at 2954 cm⁻¹ which can be assigned to -CH₂ stretching vibration. Peaks at 1602 and 1412 cm⁻¹ were observed due to the C=C stretching vibrations. Peak located at 764 cm⁻¹ was attributed

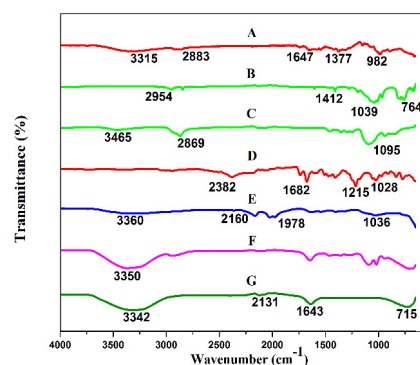


Fig. 1. FTIR spectra of A) CS, B) VTMS, C) PEG, D) DTZ, E) VTMS-g-CS, F) PEG@VTMS-g-CS, G) DTZ loaded PEG@VTMS-g-CS

to Si-O-Si symmetric stretch. The IR spectrum of PEG was observed as reported in the literature [3]. DTZ contains two carbonyl groups, as evident from the sharp peaks at 1680 and 1739 cm⁻¹. Grafting VTMS onto the primary amino groups of CS yielded low intensity peaks at 3360 cm⁻¹ due to the unreacted -CH₂ and N-H stretching vibrations. Broad band around 1036 cm⁻¹ in the copolymer was due to Si-O stretching vibration of VTMS. CAN mediated reaction yielded 92.0 % grafting efficiency indicative of the high yield of free radical initiated chain grafting. In PEG coated sample, a broad peak around 3350 cm⁻¹ was obtained which may be due to the large number of hydroxyl stretching vibrations present in PEG and CS. Broad peak observed was due to high intermolecular interaction and hydrogen bonding between functional groups of the copolymer and PEG. In DTZ loaded sample, the absorption band at 3465 cm⁻¹, concerned with C-H stretching vibration of DTZ broadened and shifted to a lower wave number of 3342 cm⁻¹ which may be due to the hydrogen bonding interaction of DTZ with the copolymer.

XRD analysis of the samples is as shown in **Fig. 2**. Characteristic peak value of PEG at 61.79° was observed, indicating its amorphous nature. In DTZ loaded sample, peaks were obtained at 21.43 , 35.59 , and 60.73° . The decrease in sharpness of the peak further confirmed the amorphous nature which may be due to the occlusion of DTZ by intercalating the linear chains of the grafted copolymer.

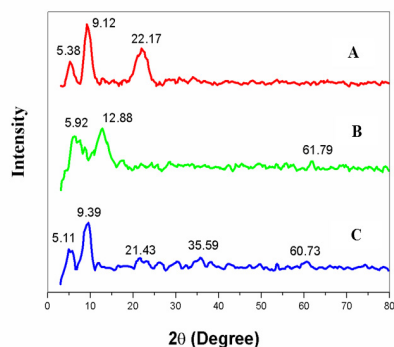


Fig. 2. XRD patterns of A) VTMS-g-CS, B) PEG@VTMS-g-CS and C) DTZ loaded PEG@VTMS-g-CS

Surface morphologies of the copolymer, DTZ loaded copolymer and the drug loaded copolymers dispersed in different matrices were observed using SEM (**Fig. 3**). VTMS-g-CS exhibited a rough and porous nature. The change from fiber like networks of CS to rough morphology was indicative of the chemical bonding between Si-CH=CH₂ groups that prevents linear stacking of CS chains. However, by employing hydrophilic coating, the surface roughness was slightly reduced with increasing amorphous nature due to the surface hydrophilicity of the PEG coated copolymer. DTZ loaded polymer showed a good dispersion of drug particles in the polymer matrix with a particle size less than 10 μm . Particle size of the drug loaded

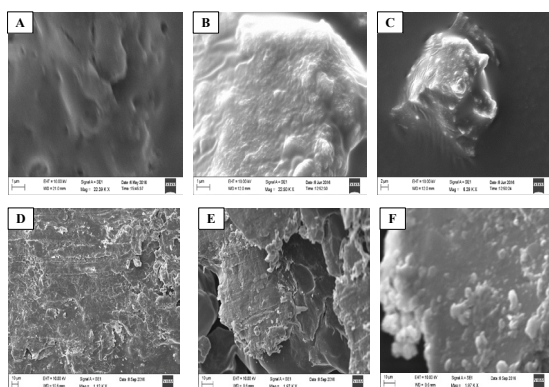


Fig. 3. SEM images of A). VTMS-g-CS, B). PEG@VTMS-g-CS and C). DTZ loaded PEG@VTMS-g-CS, D). CMC film, E). Na ALG film and F). PVA film

copolymer was found to be less than 5 μm . However, when dispersed in polymeric matrix, surface morphology changed extensively. In CMC matrix, a rather uneven and flake like structure owing to the linear chain stacking of cellulose was observed (**Fig. 3 D**). On the other hand, the particles assumed sheet like structure with surface cracks when dispersed in Na ALG matrix (**Fig. 3 E**). The surface

crack was a clear indication for the heterogeneous nature of the film. When dispersed into PVA matrix (**Fig. 3 F**), surface morphology changed to an amorphous nature with greater surface area thereby getting benefit of better contact area and controlled release.

3.2. Swelling studies

Fig. 4 depicts the swelling behaviour of PVA, SA and CMC films at pH 5.5 and 7.4 calculated using equation 1. Of the various matrices employed, CMC film exhibited highest swelling capability at both 5.5 and 7.4 pH indicating its quicker water uptake and hydration than SA and PVA films. Importantly, as desired in TDDS, PVA exhibited minimal swelling making it an ideal candidate for DTZ delivery.

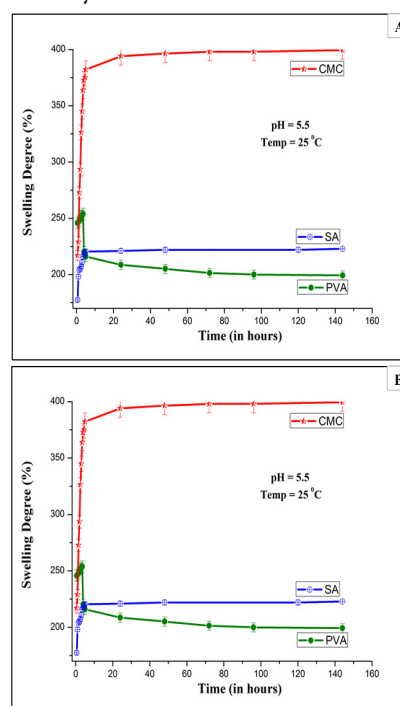


Fig. 4. Swelling degree % of CMC, SA and PVA film matrix at A). pH 5.5 and B). pH 7.4

3.3. *In vitro* permeation profile

In vitro permeation study observed at pH 7.4 is as shown in **Fig. 5**. Concentration of the copolymer was 0.0375 g/mL. The drug loading and encapsulation efficiency % were calculated as 16.0 % and 86.0 % respectively. From the permeation graph, it could be seen that 23.4 % of the loaded DTZ permeated across the rat skin. After 24 h, the amount increased to 68.9 % confirming the sustained release capability of the copolymer and then

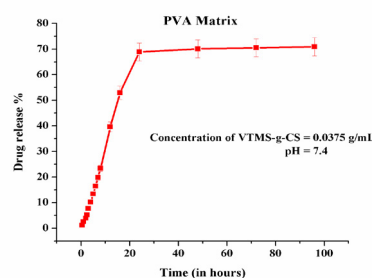


Fig. 5. *In vitro* permeation study of DTZ loaded copolymer dispersed in PVA film matrix

remained almost a constant. Even after vigorous stirring for 96 h, the amount reached only to 70.9 %, pointing out the fact that some amount of DTZ was trapped inside the porous cavity of PVA which could not be released. This might be a consequence of strong interactions between the drug and the polymeric matrix. According to calculations, the fabricated film could elute 0.0248 g of DTZ after 24 hours. Hydrophilicity offered by the PEG coating of the copolymer could significantly improve drug loading. In addition, the barrier presented by the polymeric matrix could offer sustained release.

3.4 Histological analysis

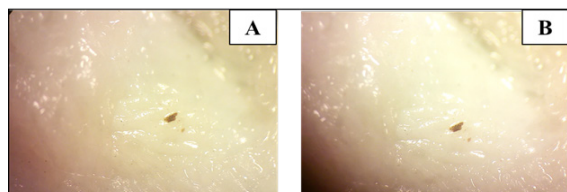


Fig. 6. Optical photos of A). Untreated skin sample and B). rat skin after 24 hour treatment with PVA film matrix

Safety of the prepared TDDS was evaluated using *in vivo* skin irritation and rat skin analysis (**Fig. 6**). After applying the PVA film on rat dorsal skin, optical photos after 24 h were taken. As seen in **Fig. 6B**), there was no area of dark patches as would be normally observed on skin irritant samples. This experiment could clearly demonstrate the non-toxicity of the copolymer and film matrix. In addition, as the treated skin looked similar to

References

1. Yadav A, Awasthi A & Rao NK, Eur. J. Med. Chem. 44 **2009**, 1-6.
2. Anirudhan TS, Nair SS, Nair AS, Carb Polm. 152 **2016**, 687–698.
3. Shameli K, Ahmad MB, Jazayeri SD, Sedaghat S, Shabanzadeh P, Jahangirian H, Mahdavi M, Abdollahi Y, Int. J. Mol. Sci. 13 **2012**, 6639-6650.

the untreated skin, the biocompatibility of the present strategy for eluting DTZ could also be confirmed.

4. Conclusions

Film forming polymeric matrix are a novel approach in TDDS and the aim of the present work was to explore the controlled transdermal release of DTZ with a view to identify and understand the various parameters that influence transdermal drug release. For achieving this, a novel hydrophilic polymer of PEG@VTMS-g-CS was synthesized and well characterized and results proved successful reaction strategies. The swelling degree of the copolymer and its dispersed polymer matrix was evaluated and the results suggested lesser swelling capability. *In vitro* permeation of DTZ across rat skin showed optimum results for PVA film. Further, histological studies on rat skin demonstrated the biocompatibility and physiological acceptance of the fabricated film. To conclude, the present strategy for the preparation of the films helps in improving DTZ therapy by assuring better drug encapsulation and sustained release with substantial physiological acceptance.

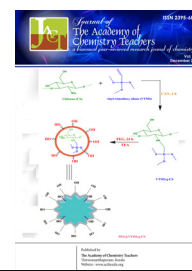
Acknowledgements

The authors are thankful to Professor and Head, Department of Chemistry, University of Kerala, Trivandrum, India for providing the laboratory facilities. One of the authors is grateful to Kerala State Council for Science Technology and Environment (KSCSTE), for providing assistance in the form of a research fellowship for this work.



Vol: 2(2) December 2016

Journal of the Academy of Chemistry Teachers



Investigation of the Morphology, Structure, Thermal and Electrical Property of Co/Ni Mixed Oxide Blended Polyaniline

Asha Bhanu A.V

Department of Chemistry, Sree Narayana College for Women, Kollam, Kerala, India - 691001

*Author for correspondence

E-mail: ashasreegowri@gmail.com

Abstract

In situ polymerization of aniline hydrochloride was carried out in presence of nickel nitrate and cobalt nitrate to synthesize PANI/Co-Ni mixed oxide composites. The surface morphology of the prepared oxide and the composite were studied using SEM, EDAX and the crystallinity were studied using XRD results. The FTIR results reveals the presence of PANI, Cobalt and Nickel oxides. The absorption shift due to the formation of the PANI composite has been studied from the UV results. Cyclic voltammetry studies explains the electro catalytic activity of the prepared PANI/Co-Ni oxides.

Keywords: PANI composites, morphology, cyclic voltammetric studies

1. Introduction

Conducting polymers plays an important role in the field of high density magnetic recording, catalysis, magnetic resonance imaging, energy conversion etc¹. Among the conductive polymers such as polyaniline(PANI),² polypyrrole³, polythiophene. PANI is considered the most promising material because of its high capacitive characteristic, low cost, and ease of synthesis.^{4,5} The metal nano particles can be incorporated in to the polymer matrix by different methods which become a field of interest for materials engineering⁶. There are four different approaches to synthesize polymer metal nano composites. The first approach is the reduction of metal salts in the polymer matrix⁷. The second method is polymerizing the organic monomer around the preformed metal nanoparticles.⁸ The third approach is the blending of preformed nanoparticles into a pre-synthesized polymer⁹. The fourth procedure is the most desirable approach in order to achieve an intimate contact between the metal and the polymer, and it involves the blending of a monomer and a metal salt.¹⁰ Nickel (II) oxide is a notable and well-studied material among various transition metal oxides because of its unique advantage in terms of properties and applications such as p-type transparent conducting film, electrochromic devices, gas sensors, spin valve devices, cathode in alkaline batteries¹¹ Song and co-workers have prepared PANI/NiO nanoparticle, nanobelt and nanotubes in the presence of sodium dodecylbenzenesulphonate which showed improved conductivity and thermal stability¹²⁻¹⁴. Nanocrystalline Co₃O₄ was found to have interesting magnetic, optical field emission and electrochemical properties which are attractive in device applications¹⁵. Co₃O₄ belongs to the normal spinel structure of AB₂O₄

type, in which Co²⁺ ions occupy the tetrahedral 8a sites and Co³⁺ ions occupy the octahedral 16d sites in the crystal lattice. In bulk crystalline form Co₃O₄ exhibits antiferromagnetism with Neel temperature of about 40K, whereas nanosized Co₃O₄ shows weak ferromagnetism or super paramagnetic properties.¹⁶ With the above background PANI/Co-Ni mixed oxides have been prepared by sol-gel route by encapsulating Cobalt oxide /Nickel oxide nanoparticles with PANI matrix by an in situ polymerization. The present investigation reports the results of extensive studies on synthesis, structural and surface characterization of nano-crystalline Cu-Ni mixed oxide systems by a variety of techniques including Fourier transform infrared (FTIR), X-ray diffraction (XRD), electron microscopy(SEM- EDAX), UV-Visible spectroscopy and cyclic voltammetry(CV).

2. Materials and Methods

All the chemicals and reagents used were of analytical grade. Cobalt nitrate, Nickel nitrate aniline hydrochloride, ammonium persulphate, acetone ethanol were purchased from Merck Ltd

All the chemicals and reagents used were of analytical grade, copper (II) nitrate, aniline, ammonium persulfate (NH₄)₂S₂O₈, acetone, ethanol, ammonia solution was purchased from Merck Ltd, and conc. HCl from SD Fine Chemicals. Double distilled water was used throughout this work.

2.1 Synthesis of Co/Ni mixed oxide

Cobalt/Nickel mixed oxide were prepared by simple sol-gel process in which 0.1M Nickel nitrate and 0.1M Cobalt nitrate were added separately to 100 ml starch solution and the mixture was magnetically stirred for one hour. Then ammonia solution was added dropwise

in the solution with constant stirring. The colour of the solution changed to bluish green. After complete addition of ammonia the solution was allowed to settle overnight and then filtered, washed using deionized water and ethanol to remove the impurities and then dried at 90°C in hot air oven. The colour of the sample changed from bluish green to dark grey at 100-850°C. The resultant mixed oxide was used for the preparation of composite using PANI.

2.2 Synthesis of PANI/ Co-Ni mixed oxide

The synthesized mixed oxide were incorporated in PANI matrix by in-situ chemical oxidative polymerization¹⁷ 0.1 M aniline hydrochloride in deionized water was kept in the ultrasonicator in ice cold water and 10 ml of prepared mixed oxide was added and again sonicated for 1 hour and then 0.1 M $(\text{NH}_4)_2\text{S}_2\text{O}_8$ (APS) was slowly added dropwise to well dispersed suspension mixture for 2 hours with continuous stirring. The conductive

emeraldine salt (ES) form of PANI/Co-Ni mixed oxide nanocomposite was obtained. After 3 hours a good degree of polymerization was done and the resultant precipitate was washed with ethanol and deionized water and dried at 60°C for 24 hours and the composite of Co-Ni mixed oxide of PANI was obtained in the powder form.

2.3 Characterization

X-Ray diffraction (XRD) analysis was carried on Bruker AXS D8 X-ray diffractometer with Cu-K α radiation ($\lambda=1.5404\text{\AA}$), with a scanning speed of $10^\circ \text{ min}^{-1}$. FTIR spectra were recorded with Aigent Gray 630 instrument in the range of 400-4000 cm^{-1} . Transmission electron microscopy images were recorded using Joel/JEM 2100 instrument. The optical absorption spectra were carried out using UV-1800 double beam UV-VIS spectrophotometer. The SEM EDAX images were recorded Bruker QUANTAX 200 and CV analysis were carried out with CHI 60646 electrochemical analyser.

3. Results and Discussion

3.1 XRD analysis

Fig :1(a) XRD of Co-Ni mixed oxide

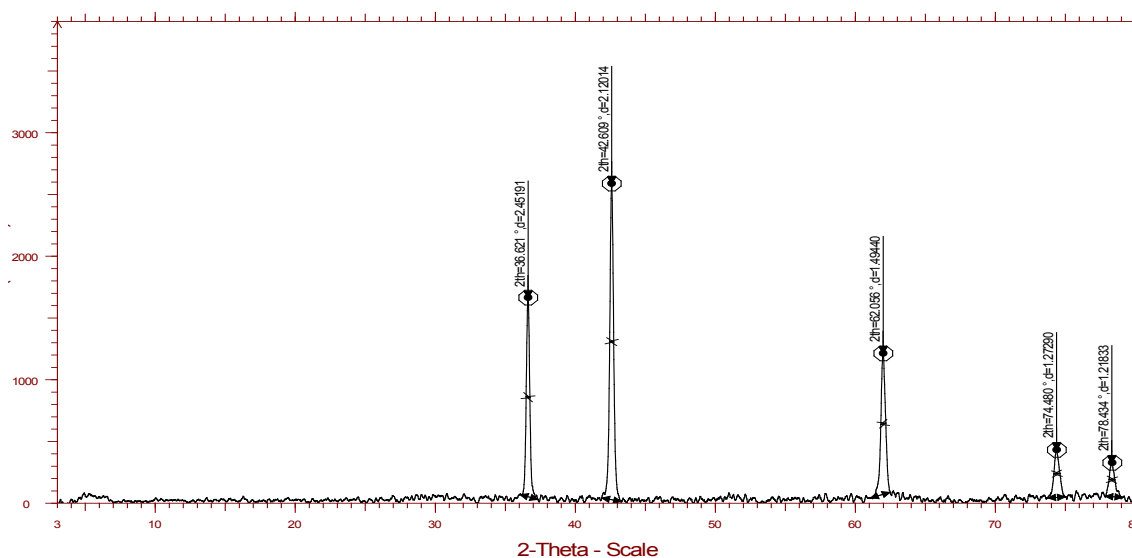
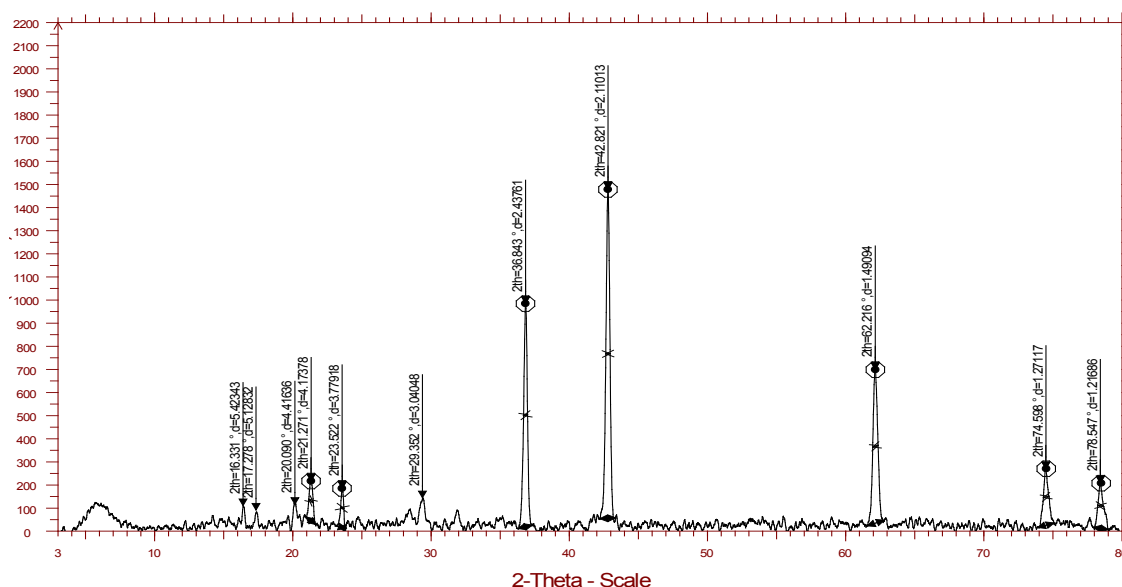


Fig 1(b) XRD of PANI/Co-Ni oxide



X-ray diffraction patterns of Co-Ni mixed oxide, PANI/NiO composites are shown in Fig 1(a) & (b). The crystalline peaks at 36.62° , 42.61° , 62.05° , 74.48° , 78.43° have been identified as peaks of single phase cubic structure of NiO and CoO with diffracting planes (111), (200), (220), (311), (222)¹⁸ matched with the JCPDS file 89-7130 and 71-1178. The crystallite size of the mixed oxide and that of the composite was found to be 39 and 48.3 nm as determined by Scherer's formula. A small hump is formed below 30° in the composite due to the periodicity parallel and perpendicular to the polymer chains which indicates the polyaniline is amorphous^{19,20}. The additional peaks at 2θ 21.26° , 23.53° clearly indicates the presence of PANI which were absent in the XRD of oxide. The XRD peaks shows the crystalline nature of the mixed oxide. This indicates that PANI undergoes interfacial interactions with the mixed oxide crystallites and the presence of mixed oxide in PANI matrix strongly affects the crystalline behavior of the formed PANI.

3.2 FTIR spectroscopic studies

Fig 2(a) and (b) shows the spectral details of mixed oxide and composite. The IR spectra of PANI shows the main

characteristic peaks at 3454 , 1578 , 1487 , 1307 , 1251 , 1147 and 824 cm^{-1} . The bands at 1578 and 1487 cm^{-1} are attributed to stretching vibrations of N=Q=N ring and N-B-N ring respectively (where B refers to benzenic-type rings and Q refers to quinonic-type rings)¹⁷. The peak at 824 cm^{-1} is due to the out-of-plane bending vibration of C-H on the 1,4-disubstituted aromatic rings²¹. The absorption bands due to stretching vibrations of quinoid and benzoid rings in PANI/NiO nanocomposites indicate the emeraldine form of oxidation state confirmed the polymerization of aniline in the presence of NiO. The FTIR spectra of the polymer shows peaks at 650 which is due to the presence of cobalt oxide in the polymer nano composite. For the PANI- composites its IR spectrum is almost identical to that of the pure PANI but all bands shift slightly towards red (lower frequency side), and the intensity ratio of quinonoid band has also changed. These results indicate that some interactions (kind of weak Vander Waals force of attraction) exist between PANI and the metal oxide²². Broad absorption band in the region of 631 – 772 cm^{-1} is assigned to Ni–O stretching vibration mode.

Fig 2(a) FTIR spectra of Co-Ni mixed oxide

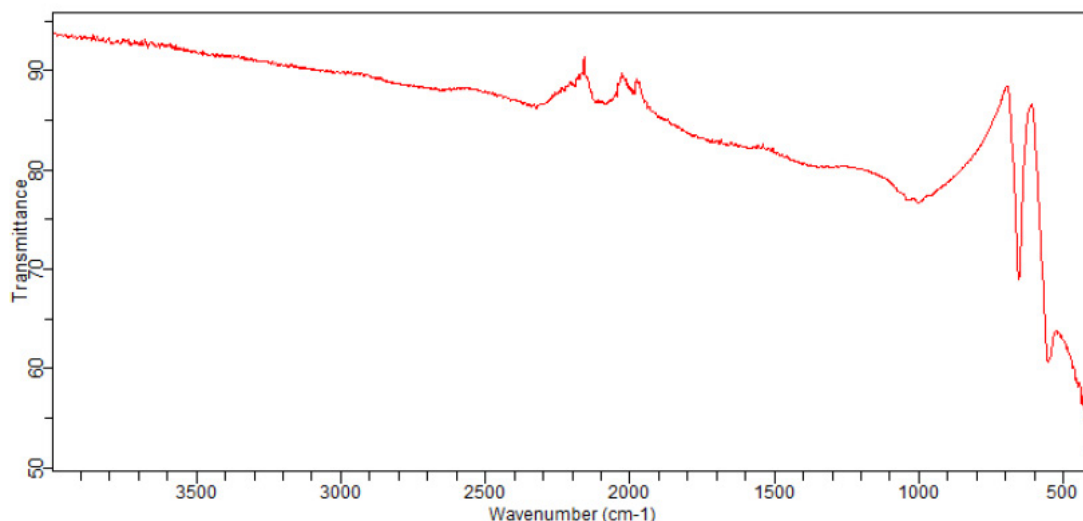
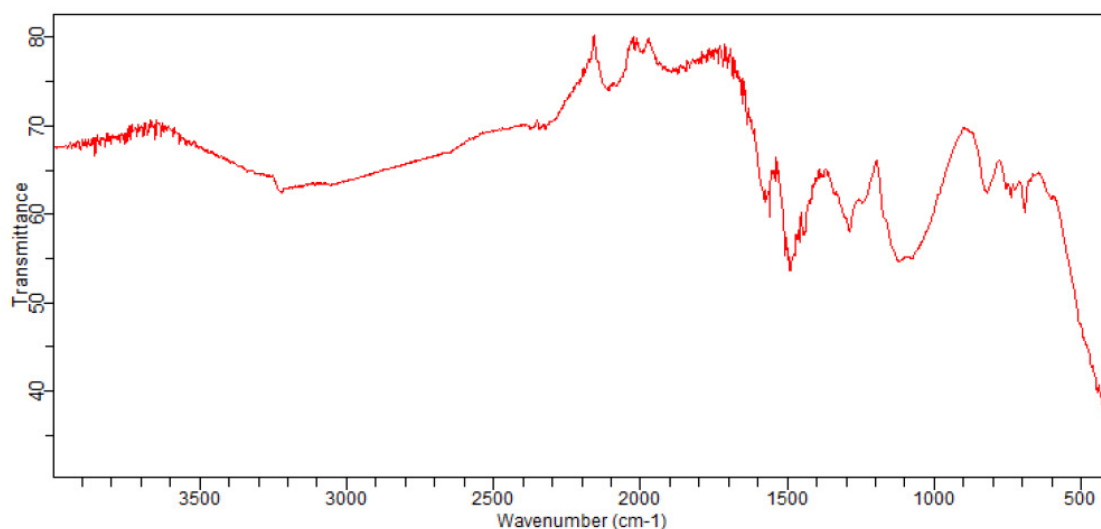


Fig 2(b) FTIR of composite of PANI/Co-Ni mixed oxide PANI



3.3 Morphology

Fig 3 (a) TEM image of Co-Ni mixed oxide

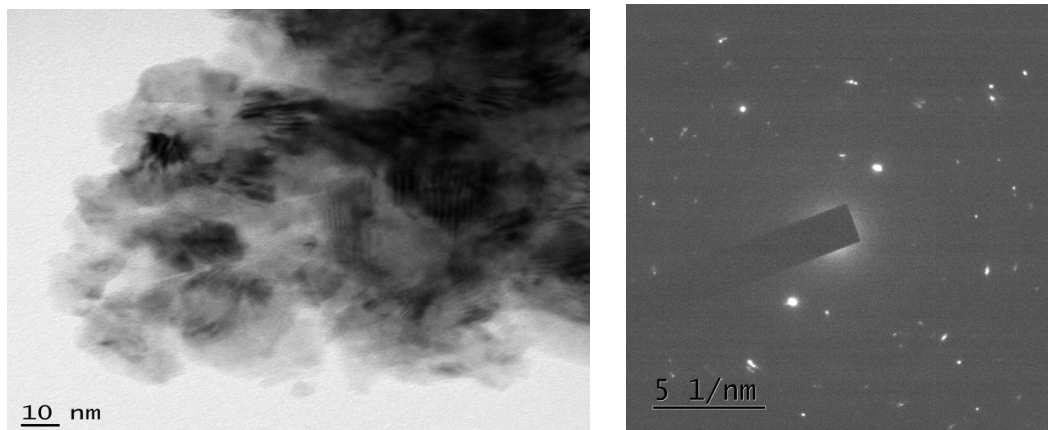
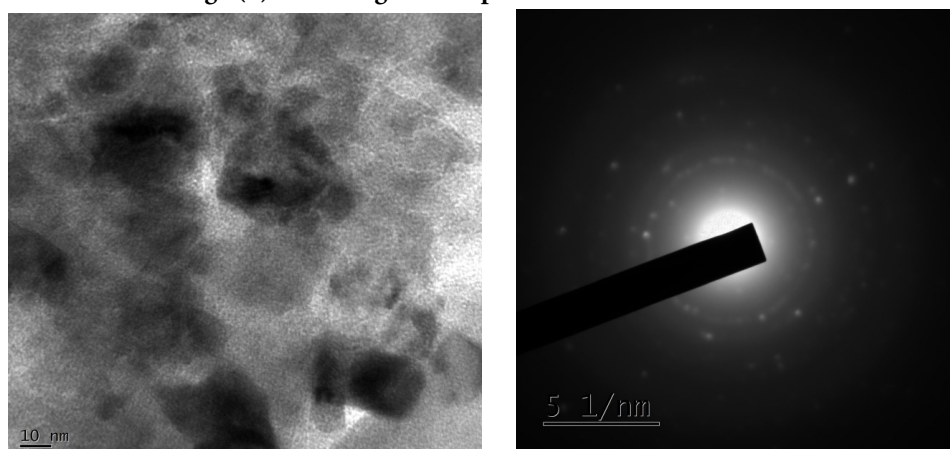


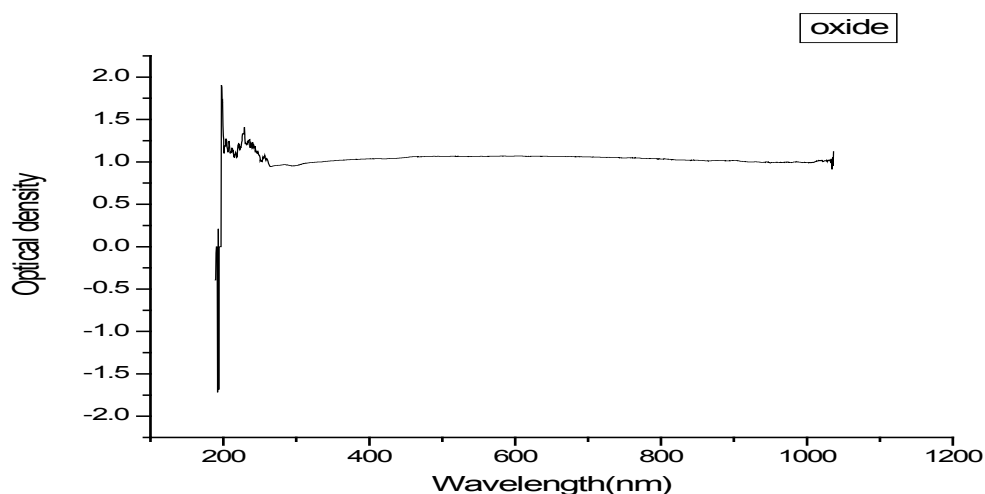
Fig 3(b) TEM image of composite of PANI/Co-Ni oxide

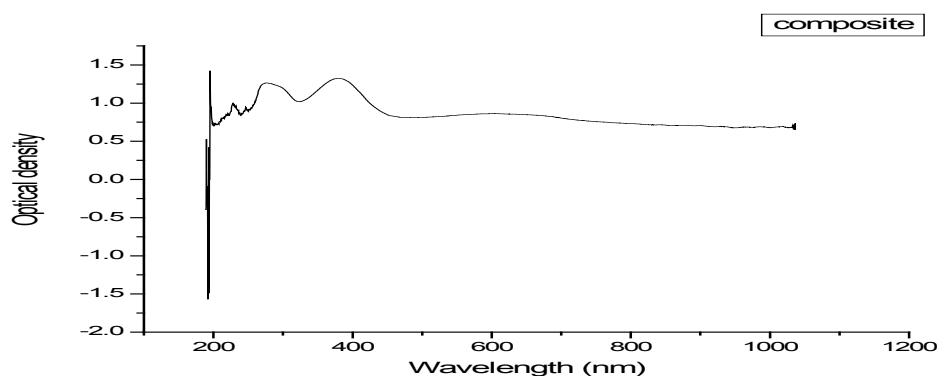


From the TEM images Fig 3(a) and (b) it is seen that Co and Ni oxide nanoparticles are mostly irregular in shape. The size of the particle range from 10 to 50nm. The oxide particles are seen to aggregate in the case of composite and they are dispersed in the polymer matrix^{23,24}. It is shown in the TEM that the dark portion are the nano particles and the grey portion is the polymer chain. So it is clear from the micrograph that the polymer molecules have been adsorbed on the surface of the nano particles. The molecules of the PANI and the particles are hence bounded by weak bonds and they are found in the composites

3.4 UV-Visible spectroscopic studies

Fig 4 UV-Visible spectroscopic studies





In the UV-Visible spectrum of the composite there is a band at 270 nm which is due to the inter band transition $\pi \rightarrow \pi^*$ of excitons in the aromatic ring. The band at 650 nm in the spectra of the composite is associated with the inter band charge transfer associated with the excitation of benzenoid to quinoid moieties (formation of an exciton – bipolaronic band) in PANI^{25,26}. The band at 420 nm due to the electronic transitions from highly occupied electron orbital which called the valance band (VB) to unoccupied electron orbital which named the conduction band (CB)²⁷.

3.5 SEM-EDAX

Fig 5 (a) SEM EDAX of mixed oxide

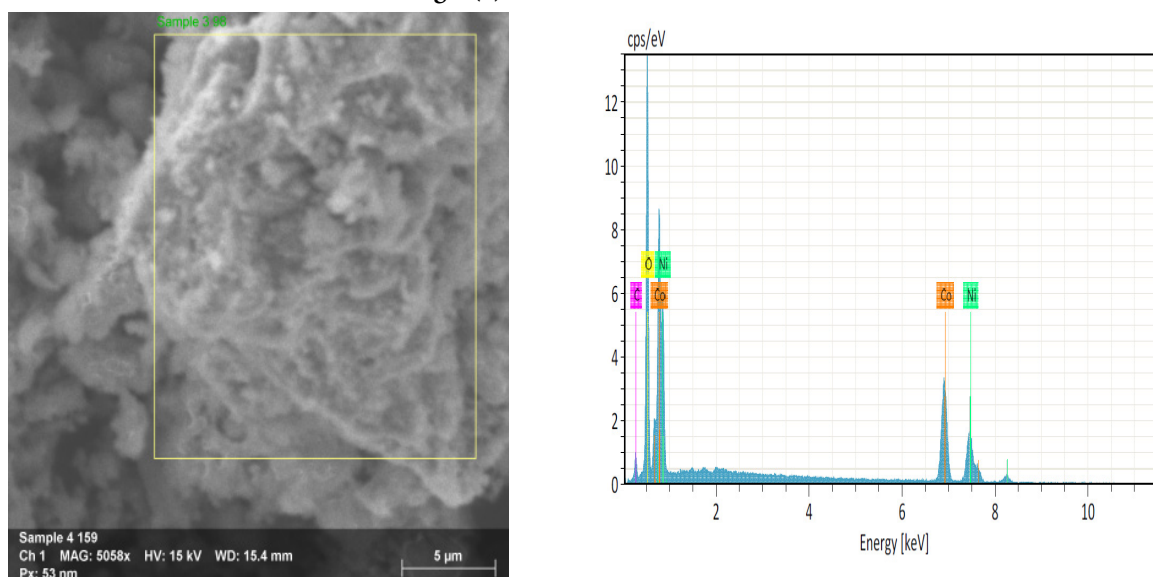
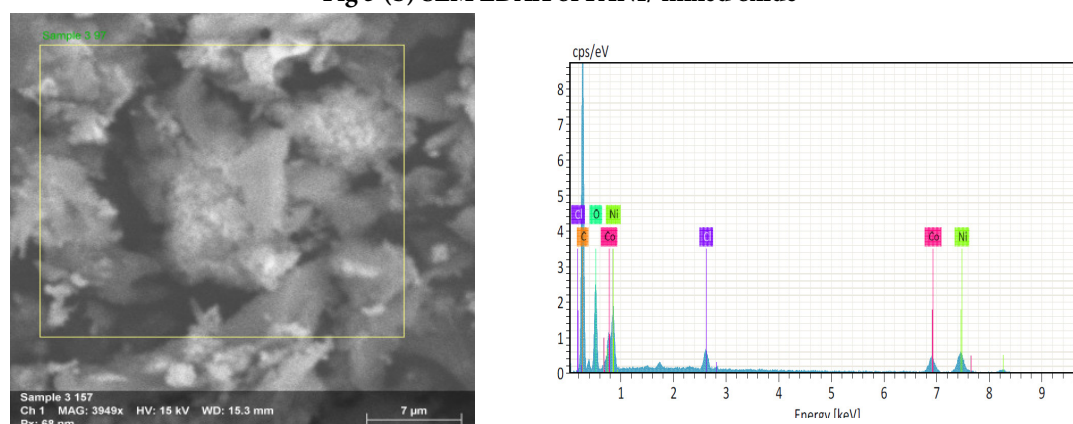


Fig 5 (b) SEM EDAX of PANI/ mixed oxide



EDAX

The Energy dispersive X-ray analysis Fig 5(a)&(b) indicates the different abundance of metal oxide in contact with the polymer matrix. The concentration of oxide particle in the polymer are different in different regions which can be a consequence of the ultrasonic treatment resulting in the non-homogeneous pattern of the oxide materials in the PANI matrix²⁸.

3.6 CYCLIC VOLTAMMETRY STUDY

Fig 6: CV of Oxide & Composite

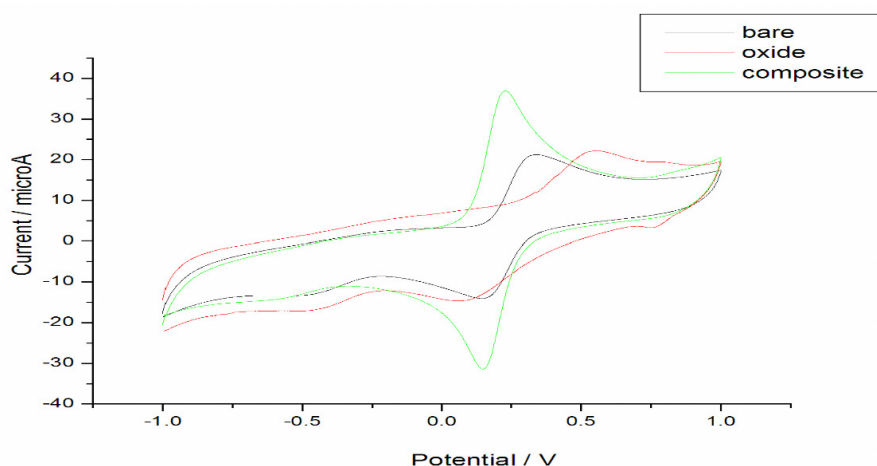


Fig 6 shows the cyclic voltammogram of the prepared oxide and the composite. The electrochemical process occurring at the oxide and composite on modified glassy carbon electrode at the scan rate of 50mVs^{-1} in $\text{K}_4\text{Fe}(\text{CN})_6$ buffer solution. A well defined peak is observed for the composite of PANI than for the bare electrode. A definite cathodic and anodic peaks are observed at 0.3V and 0.15V . The oxide and the composite undergo reversible process. The current density of the composite is increased as compared to oxide as potential decreases which indicate that composite is having good electrocatalytic activity.

Conclusion

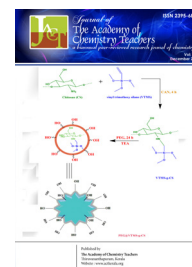
The PANI-Co-Ni nano composite have been successfully prepared by in-situ polymerization using ammonium persulphate as an oxidant. The XRD pattern of the mixed oxide and the composite reveals the face centered cubic phase of the oxide and the composite. The average particle size of the oxide and composite as calculated using Debye Scherer formula was found to be 39 and 48.3nm . From the XRD studies it is clear that

PANI undergoes interfacial interaction with the Co-Ni oxide. The TEM images clearly reveals the oxide particles are dispersed in the polymer matrix. The FTIR spectra also indicates the presence of PANI in the composite. The UV spectra shows the presence of emeraldine base form of PANI. The voltammogram behavior of composite shows that it has good electrocatalytic activity as compared to oxide.

References

1. Tartaj, P, MD Morales, Veintemillas-Verdaguer S, Gonzalez-Carreno. Tand Serna C, J J Phys D36, **2003** .182–197.
2. Cao, Y; Mallouk, T. E. Chem. Mater, 20, **2008**, 5260.
3. Wu, Q; Xu, Y; Yao, Z; Liu, A; Shi, G. ACS Nano 4(4), **2010**, 1963.
4. Liu D. Y, Reynolds J. R. ACS Appl. Mater. Interfaces, 2(12), **2010**, 3586.
5. Jang, J; Bae, J; Choi, M; Yoon, S. H. Carbon 43, **2005**, 2730.
6. Swami A; Kumar A., Selvakanna, P, Mandal, S., Pasricha, R., Sastry, M. Chem. Mater. 15, **2003**, 17.
7. Selvan S. T, Spatz J P, Klok H A, Möller M, Adv. Mater, 10, **1998**, 132.
8. Lee J, Sundar V C, Heine. R, Bawendi M G, Jensen K F, Adv. Mater, 12, **2000**, 1102.
9. Corbierre M K, Cameron N S, Sutton M, Mochrie S G J, Lurio L B, Ruhm A, Lennox R B, J. Am. Chem. Soc. 123, **2001**, 10411.
10. Mallick K, Witcomb M J, Scurrrell M S, Strydom A M, Gold Bulletin 41(3), **2008**, 246.
11. Srivastava A.K, Thota, S J Nanosci. Nanotech. 8(8) **2008**, 4111.
12. Song G.P, Han J Guo R, Synthetic Metals, 157, **2007**, 170.
13. Song, G.P, Bo J, Guo R, Colloid Polym. Sci. ,283, **2005**, 677.
14. Han J, Song G.P Guo R., J. Polym. Sci. Part Polym. Chem. 44, **2006**, 4229.
15. Bharati Nandapure, Subhash Kondawar, Mahesh Salunkhe and Arti Nandapure, Journal of Composite Materials 47(5) **2012**, 559–567. .
16. Shambharkar B H, Umare SS. Production and characterization of polyaniline/ Co_3O_4 nanocomposite as a cathode of Zn-polyaniline battery. Mater Sci Eng B 175, **2010**; 120–128.

17. Nandapure B I, Kondawar S B , Salunkhe M Y, Nandapure A I, Adv. Mat. Lett. 4(2), **2013**, 134-140.
18. Mironova-ulmane N, Kuzmin A.A, Grabis B J, Sildos I, Voronin VI, Berger I F, Kazantsev V A, Solid State Phenomena, 168, **2011**, 341.
19. Thakur B, Amarnath C.A, Mangoli S H, and Sawant S N, Sensors and Actuators, B: Chemical 207, **2014** 262–268.
20. Amarnath C.A, Venkatesan N, Doble M, and Sawant S N, Journal of Materials Chemistry B, 2(31), **2014** 5012–5019.
21. Shambharkar B.H, Umare S.S, J. Appl. Polym. Sci. 122, **2011**, 1905.
22. Mahesh D, Raghunandan Deshpande, Basavaraj Salimath, Venkataraman Abbaraju ,American Journal of Materials Science 2 (3) ,**2012**, 39-43.
23. Bahari Molla M, Y.; Sadrnezhaad S.K. and Hosseini, D, J Nanomaterials, 2008, 1-4.
24. Masoud Salavati-Niasari , Afsaneh Khansari , Fatemeh Davar, J. Inorganica Chimica Acta 362 **2009** 4937–4942.
25. Kondawar S B, Hedau M J, Tabhane VA Modern Phys Lett B 20(23) **2006**, 1461–1470.
26. Gupta M C, Warhadpande S V and Umare S S Indian J Chem 32 A, **1993** , 298–302.
27. Abdo Mohd Meftah, Elias Saion, Mohd Maarof B Hj Abd Moxsin and Hishamuddin B Zainuddin , Solid State Science and Technology, Vol. 17, **2009** 167-174
28. Mosquedaa.Y, Pe´rez-Cappea.E, Aranab.J, Longob.E, Riesb.A, Cilenseb.M.,Nascentec P, Arandad P, Ruiz-Hitzky.E Journal of Solid State Chemistry 179 **2006** 308–314.



A Comparative Study of the Ion Exchange Properties of Some Cerium (IV) Based Compounds

Apsara A. P^{a*}, Beena B^b

Department of Chemistry, Fatima Mata National College, Kollam, Kerala, India - 691 001

Department of Chemistry, DB College Sasthamcotta, Kollam, Kerala, India - 690 521

*Author for correspondence:

E-mail: apsaraap@gmail.com

Abstract

Cerium(IV) based samples namely cerium phosphate (CP), cerium molybdate (CM) and cerium phosphomolybdate (CPM) were synthesized by co-precipitation method. Ceric sulphate, ammonium heptamolybdate, disodium hydrogen phosphate were mixed to obtain a material of optimum sodium exchange capacity. The selected material was characterized by ICP-AES, XRD and FTIR in addition to chemical stability and ion exchange studies. Ion exchange capacities (i.e.c) for different alkali and alkaline earth metals and the effect of heat on i.e.c were determined. In the present work, the materials show preference for Na⁺ ion, among the alkali metals and for Mg²⁺ and Ca²⁺ ions among alkaline earth metals and have reasonably high sodium exchange capacity even at high temperatures.

Keywords: Inorganic ion exchanger, Cerium (IV) compounds, TMA salts, ion exchange capacity

1. Introduction

Insoluble salts of tetravalent metals (TMA) can be prepared both in crystalline and amorphous forms¹. They can be obtained by the combination of tetravalent metal salts with anions like phosphate, molybdate, arsenate, antimonate, tungstate etc. They have the general formula M(IV) (HXO₄)₂.nH₂O where M(IV) = Zr, Ti, Sn, Ce, Th etc and X = P, Mo, W, As, Sb etc. These compounds have structural hydroxyl groups, the H of -OH being exchangeable sites. A number of cations can be exchanged with H⁺ due to which the materials possess cation exchange properties². Such inorganic ion exchangers have multiphased applications owing to their properties such as selectivity for certain metal ions, high stability in strong acids, oxidizing solutions and ionizing radiations³. They are especially attractive for analytical applications where organic resins cannot be employed because of their degradability. Due to the presence of surface hydroxyl protons they can be successfully employed as Bronsted acid catalysts and protonic conductors^{4,5}. They can also be used as sorbents for the removal of dyes, pesticides, organic molecules etc⁶. The present study is devoted to the preparation, characterization and ion exchange properties of tetravalent cerium based materials.

2. Experimental

2.1 Preparation of samples

CP in the present study was prepared by adding an aqueous solution of disodium hydrogen phosphate to half its volume of ceric sulphate slowly, with continuous stirring at pH~2. Equimolar solutions of ammonium

heptamolybdate and ceric sulphate were mixed in the volume ratio 1:2 at pH~2, for the preparation of CM. Aqueous solution of ammonium heptamolybdate (100mL) and disodium hydrogen phosphate (200 mL) were added to an aqueous solution of ceric sulphate (100 mL), slowly with continuous stirring at pH~2 for the preparation of CPM.

In all the above cases, the gel obtained was kept overnight at room temperature in contact with the mother liquor for the growth of fine particles. The granular precipitate thus obtained in each case, was filtered, washed with demineralized water till free of chloride and sulphate ions and finally dried at 40°C. All the materials after drying were broken to desired particle size (ASTM, 30 – 60 mesh) by grinding and sieving.

2.2 Chemical stability

Chemical stability of a material plays an important role for it to be used as an ion exchanger. The stability of the exchangers were checked in different acids like HCl, H₂SO₄, HNO₃, bases like NaOH & KOH, organic solvents like ethanol, diethyl ether, acetic acid and in 1M salt solutions of alkali and alkaline earth metal chlorides. In each case, 500 mg of the ion exchanger was taken in 50 mL of the particular solvent and kept for 24 h. The change in colour, nature and weight was observed in each case.

2.3 Characterization

Elemental analysis of the compound was obtained from Thermo Electron IRIS Interpid II XSP Duo, ICPAES

Spectrometer. X-Ray diffractograms were taken from Bruker D8 Advance diffractometer using Cu K α radiation. FT-IR spectrum was recorded on a Perkin Elmer Fourier Transform Spectrometer. Thermograms of the samples in the present study were taken with Perkin- Elmer Diamond Thermo Gravimetric Analyzer at a heating rate of 10°C per minute in N $_2$ atmosphere.

Ion Exchange capacity (i.e.c) of the material was determined by column method⁷. To study the effect of heat on i.e.c, the samples were heated to the respective temperature in a muffle furnace, cooled to room temperature and i.e.c of the material was then determined by column method.

3. Results and Discussion

CP was obtained as a pale yellow solid. CM was a hard bright orange solid while CPM was a bright yellow powder. The materials showed no change in colour or form on heating with water. They were found to be stable in mineral acids like HCl, H $_2$ SO $_4$ and HNO $_3$ upto ~7 M concentrations as evidenced by no change in colour, form or weight of samples used. In higher concentrations of acids leaching of cerium was observed. The ion exchangers CM and CPM were found to be unstable in higher concentrations of bases like NaOH and KOH (above 6M) where they turned white in colour, may be due to hydrolysis. However, CP was found to be stable in all concentrations of bases. All the materials were also found to be stable in ethanol, diethyl ether, acetic acid and 1 M salt solutions.

Elemental analysis shows that CP contains 38.36% of cerium and 16.29% of phosphorous. The percentage of cerium and molybdenum in CM was found to be 17.28 and 41.65% respectively. CPM was found to contain 5.88% of cerium, 3.99% of phosphorous and 41.7% of molybdenum. The amorphous nature of the materials namely CP and CM is evident from the absence of strong peaks in the X-ray diffractograms as seen in Fig 1. The sharp peaks in the XRD of CPM confirmed the presence of nanocrystallites. The Debye- Scherrer formula has been used to calculate the crystallite size⁸. The crystallite size was calculated and was found to be 36nm for CPM.

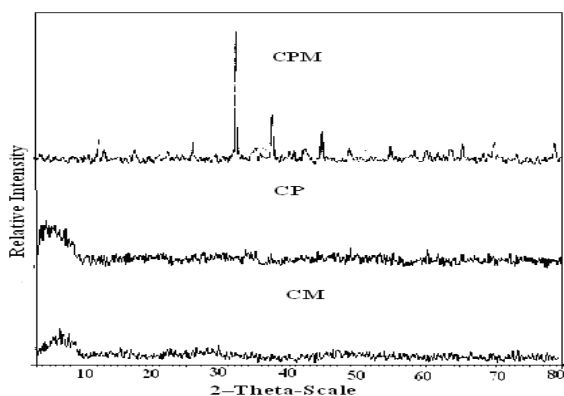


Fig. 1 - XRD of CP, CM and CPM

The thermograms of CP and CM (Figs 2a, 2b respectively) show sharp change in weight around 100°C

corresponding to the loss of external water molecules and a small weight loss between 200 - 400°C due to the removal of co-ordinated water molecules after which a gradual loss in weight is observed till 800°C. This may be due to the condensation of structural hydroxyl groups, which is the usual behaviour of inorganic ion exchangers⁹. TG of CPM (Fig. 2c) also shows a similar behavior.

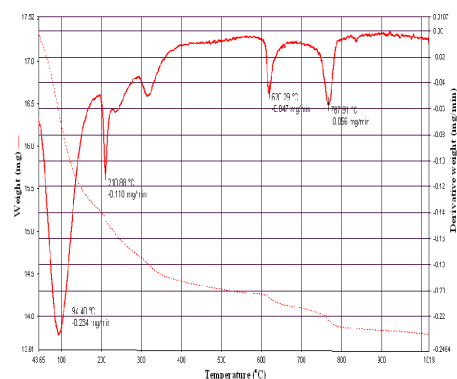


Fig. 2a TGA-DTA of CP

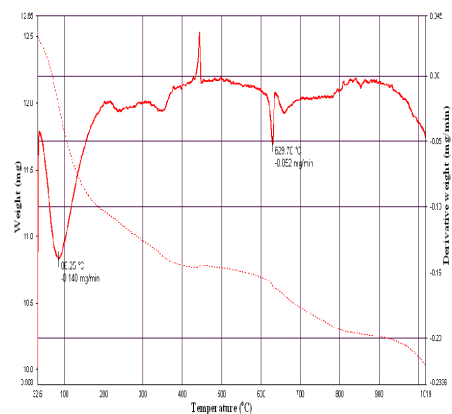


Fig. 2b TGA-DTA of CM

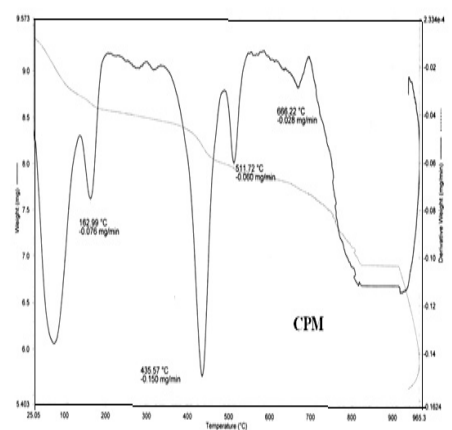


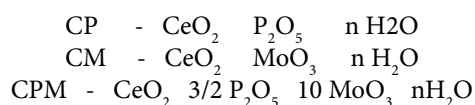
Fig. 2c TGA-DTA of CPM

According to TG data, CP loses 15% of its total mass in the temperature range 43- 300°C while CM shows 12% weight loss in the same temperature range. It is apparent from the curve that CPM suffers a weight loss of 7.5% in the temperature range 100-200°C due to loss of moisture/hydrated water. The weight remains constant in the

temperature range 200-400°C. On further increasing the temperature (400-500°C), CPM shows a weight loss of 2.4% which is attributed to the condensation of structural hydroxyl groups. DTA of the materials also shows endothermic peaks corresponding to these changes. A phase transition accompanying dehydration is seen as an exotherm around 450°C in the DTA curve of CM.

Elemental analysis data gives the percentage composition of different elements in the material, from which the empirical formula can be calculated by usual methods¹⁰. The prepared samples contain varying amounts of water molecules. It is assumed that the water molecules are lost on heating, resulting in the formation of anhydrous mixed oxide at high temperatures.

Therefore, based on elemental analysis, the following empirical formulae were proposed for CP, CM and CPM.



The number of external water molecules 'n' in these compounds, were further calculated from TGA data using Alberti and Torracca formula¹¹.

$$18n = X (M + 18n) / 100$$

M = molecular weight of the exchanger without water molecules

X = percentage weight loss upto 180° C

Based on the above formula it is found that n = 2 in CP, 5 in CM and 8 in CPM

The FTIR spectra of all the materials show bands around 3300 cm⁻¹ corresponding to the vibrations of O-H as well as Ce(OH)₂²⁺ group (681 – 553cm⁻¹). The spectrum of CP shows bands representative of P-OH group (1068 cm⁻¹) while CM shows bands characteristic of molybdate ion (824 cm⁻¹) and CPM shows the presence of peaks corresponding to P-OH (1064 , 968 cm⁻¹) as well as molybdate ion (860 – 794 cm⁻¹)¹². CP, CM and CPM

possess structural –OH groups responsible for their ion exchange behaviour which is also evident from their i.e.c values.

The Na⁺ exchange capacity of CPM was found to be 7.00 meq/g where as for CP and CM it was found to be 2.26 and 5.08 meq/g respectively. The exchange capacities with other alkali and alkaline earth metals taken as their respective chloride salt solution (1M) are summarized in Table 1. The selectivities for alkali metal ions indicate that the i.e.c of CP, CM and CPM is independent of the size of the ingoing hydrated ion. Inorganic ion exchangers unlike their organic analogs, usually have rigid structures and do not undergo any appreciable change during ion exchange. The rigid structure leads to specific and unusual selectivities¹³. The size of the cavities within the exchanger depends on the composition and water of hydration of the ion exchanger¹⁴. In the present work, the materials show preference for Na⁺ ion, among the alkali metals studied. TMA salts with high affinity for Na⁺ ions were reported by other workers also¹⁵.

The preference for Na⁺ ions may be due to the following reasons¹⁶:

- Partial dissociation of the anionic groups in the material
- Formation of cavities of proper dimensions for Na⁺ ion
- Basic dehydration involving primary hydration shells of Na⁺ ion

In general, alkaline earth metal ions have high i.e.c values than alkali metal ions. In the case of monovalent ions, when they are exchanged with H⁺ type exchanger, no net numerical changes take place between incoming and releasing ions.

In contrast, when divalent ions are exchanged with the exchanger, the number of releasing ions is twice as much as the incoming ions. This may bring an increase in overall entropy change and hence accounts for the high i.e.c values with M²⁺ ions as compared to M⁺ ions¹⁷.

Table 1 - Exchange capacities for alkali and alkaline earth metal ions on CP, CM and CPM

Metal ion	Ionic radii (A ⁰)	Hydrated ionic radii (A ⁰)	Ion exchange capacity (meq/g)		
			CP	CM	CPM
Li ⁺	68	600	1.68	0.53	4.81
Na ⁺	97	450	2.26	5.08	7.00
K ⁺	133	300	1.73	1.27	3.52
Mg ²⁺	66	800	4.60	10.60	13.36
Ca ²⁺	99	600	2.59	4.24	8.43
Sr ²⁺	112	500	3.73	0.42	6.13
Ba ²⁺	134	450	1.07	0.40	8.02

Table 2- Effect of heat on Na⁺ i.e.c of CP,CM and CPM

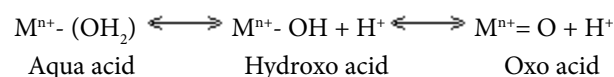
Temperature(°C)	CP		CM		CPM	
	i.e.c(meq/g)	colour	i.e.c(meq/g)	colour	i.e.c	colour
RT	2.26	Paleyellow	5.08	Brightorange	7.00	Yellow
100	1.13	Cream	5.65	Orange red	8.20	Yellow
200	0.67	Cream	5.65	Orange red	8.63	Yellow
300	0.45	Cream	5.65	Orange red	7.11	Yellow
400	0.20	White	2.45	Cream	1.47	Blue
500	0.20	White	1.13	Cream	10.61	Bluegreen

RT – Room Temperature

Among the alkaline earth metals CP, CM and CPM shows preference for Mg²⁺ ion. Water molecules of metal ions having small ionic radius may be tightly bound by coulombic field of the metal ion. Mg²⁺ ion with a small ionic radius is strongly hydrated in aqueous solution. Thus, it is anticipated to be exchanged with its hydration shell being constant. Therefore, Mg²⁺/ H⁺ exchange may contribute to the net transfer of water molecules from the aqueous phase to the exchanger phase¹⁸.

The effect of heating on i.e.c of the materials given in Table 2 reveals that, for CP it decreases on heating. But for CM the exchange capacity initially increases, remains constant up to 300°C and then decreases on heating. The initial increase in i.e.c on heating may be due to removal of adsorbed water thereby activating the exchanger. The decrease in i.e.c observed for both CP and CM at higher temperatures is attributed to the condensation of structural hydroxyl groups¹⁹. The colour change of CP from cream to white is an indication of the reduction of Ce(IV) to Ce(III)²⁰. CPM shows an abnormal variation in i.e.c on heating (Table 2). The i.e.c shows an increase on heating the material to 200°C after which a decrease is observed at 300 and 400°C followed by a sudden increase at higher temperatures. The high exchange capacity of CPM heated to higher temperatures can

also be attributed to the formation of respective oxides at high temperatures. These oxides when hydrated show acid properties due to the dissociation of water molecules connected co-ordinatively with the polycharged cations, at higher temperatures, forming aqua hydroxo complexes and protons, as represented below²¹.



4. Conclusion

All the cerium based ion exchangers in the present work show high affinity for Na⁺ ions among the alkali metals studied. Such materials with high selectivity for Na⁺ find application in electro-deionization which is a desalination method based on a combination of ion exchange resin and ion exchange membrane. They also find application in the removal of sodium from natural and industrial brines in a reasonable period. Among the alkaline earth metals studied, the ion exchangers in the present study show high affinity for Mg²⁺ and Ca²⁺ ions. Therefore, these ion exchangers may also be used in the removal of hardness of water. The ion exchangers studied in the present work are stable with reasonably high sodium exchange capacity even at high temperatures.

References

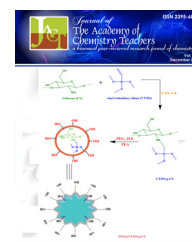
1. Clearfield A (Ed.), Inorganic Ion Exchange Materials, CRC Press, Inc Boca Raton, Florida. **1982**
2. Pillay K K S Radioanal. Nucl. Chem., 102, **1986**, 247-268.
3. Mu Naushad, Ion Exch. Lett. 2, **2009**, 1-14.
4. Beena B and Chudasama U, Indian J. Chem. Tech., 2, **1995**, 339-340
5. Abraham Clearfield, Chem. Rev., 88, **1988**, 125-148.
6. Apsara AP and Beena B, IJEP, 35(4), **2015**, 294-299.
7. Weqar Ahmad Siddiqui, Shakeel Ahmad Khan, Bull.Mater.Sci., 30, **2007**, 43-49.
8. Culyty B D and Steck S R, Elements of X-ray Diffraction, 3rd Edition, Prentice Hall, Englewood Cliffs, NJ, **2001**
9. Michael E Brown (Ed.), Introduction to thermal analysis: Techniques and applications, 2nd Edn., Kluwer Academic Publishers, Netherland, **2001**
10. Shriner R L, Hermann C K F, Morrill T C, Curtin D Y and Fuson R C, *The systematic identification of organic compounds*, 7th Edn. John Wiley & Sons, Inc. New York, USA, **1998**
11. Alberti G and Torracca E, J Inorg Nucl Chem, 30, **1968**, 3075-3080
12. Socrates G, *Infrared Characteristic Group Frequencies*, Wiley, NJ, **1980**

13. Helfferich F, *Ion Exchange*, McGraw-Hill, New York, **1962**
14. Qureshi M, Rathore H S and Kumar R, , J Therm Anal, 3, **1971**, 371-378
15. Nilchi A, Maalek B, Khanchi A, Marageh M G and Bagheri A, Radiat Phys Chem, 75, **2006**, 301-308
16. Nabi S A, Naushad M and Inamuddin, J Hazard Mater., 142, 2007, 404-411
17. Rawat J P and Thind P S, J Indian Chem Soc, 57, **1980**, 819
18. Varshney K G, Singh R P and Uma S, Colloids and Surfaces , 16, **1985**, 207-218
19. Abd El-Latif M M and Elkady ME, Mater Res Bull, 46, **2011**, 105-118
20. Alberti A, Costantino U, Gregorio F D and Galli P, J Inorg Nucl Chem, 30, **1968**, 295
21. Gopalakrishnan J and Rohini Mani, J Chem Sci, 121, **2009**, 235-256



Vol: 2(2) December 2016

Journal of the Academy of Chemistry Teachers



Synthesis and Characterization of Tetraaquafumaratozinc(II): A 1D MOF with Supramolecular Assembly

Dhanya V.S, Sudarsanakumar M.R*

Department of Chemistry, Mahatma Gandhi College, Thiruvananthapuram, Kerala, India - 695 004

*Author for correspondence:

E-mail: sudarsanmr@gmail.com

Abstract

A supramolecular framework system tetraaquafumaratozinc(II) (TAFZ) was grown successfully by single gel diffusion technique at room temperature. Good quality transparent single crystals have been obtained in 15 days. The crystalline nature and reflection planes of the sample were confirmed by the powder X-ray diffraction technique. The crystal structure was determined by single crystal X-ray diffraction technique and consists of 1D chain. The coordinated water molecules take part in hydrogen bonding and form a supramolecular framework. Fourier Transform Infrared (FT-IR) studies were used to confirm the presence of various functional groups in the compound. The thermal behavior of the crystal was studied by TGA in nitrogen atmosphere.

Keywords: Crystal growth, Gel diffusion technique, Supramolecular Framework, Thermal studies

Introduction

Supramolecular chemistry has developed over the last few years as chemistry beyond the molecule¹. Starting with the investigation of the basis of molecular recognition, it has explored the implementation of molecular information in the programming of chemical systems towards self-organisation processes that may occur either on the basis of design or with selection of their components. Supramolecular entities are by nature constitutionally dynamic by virtue of the liability of non-covalent interactions. Fumaric acid as a dicarboxylic acid has variable coordination modes making it suitable for the construction of MOFs with supramolecular assemblies^{2,3}.

In this work the growth and characterization of tetraaquafumaratozinc(II) (TAFZ) with supramolecular assembly has been described. The crystal structure of the compound is reported earlier⁴ by hydrothermal synthesis. Herein we present the growth of the title compound using single gel diffusion technique at room temperature and more insight into the crystal structure. To the best of our knowledge this is the first report of the title compound using silica gel method. The crystals were characterized by elemental analysis, FT-IR and UV-visible spectral studies. Thermal decomposition behavior was analyzed by TGA. Single crystal X-ray diffraction studies elucidated the crystal structure of the compound.

Experimental procedure

The crystallization of TAFZ was accomplished using single gel diffusion technique using sodium metasilicate (5). The crystallization apparatus is borosilicate glass tube of length 20 cm and diameter 2.5 cm. The gel was prepared

by adding a solution of sodium metasilicate of desired density (1.02-1.04 g cm⁻³) to fumaric acid of desired molarity (0.125-1 M) drop by drop with continuous stirring. A fixed amount of gel solution with the desired value of pH (3-8) was then transferred to several glass tubes. After setting the gel, an aqueous solution of zinc sulphate (upper reactant) of desired molarity (0.125-1 M) was added slowly along the walls of the tube without tampering the gel surface. The top of the glass tubes were covered with transparent sheet of plastic and then kept in a wooden stand.

1. Characterization

The carbon and hydrogen contents in the obtained crystals were determined by using Elementar Vario-EL 111 CHNS analyzer. The powder X-ray diffraction studies were conducted using a Bruker AXS D8 advance XRD with Cu K α radiation ($\lambda = 1.54056 \text{ \AA}$). The FT-IR spectrum was recorded on potassium bromide pellets on a Thermo Nicolet, Avatar 370 spectrometer in the range 4000-400 cm⁻¹. The absorption spectrum of the crystals was studied using Varian Cary 5000 UV-visible-NIR spectrometer in the range 200-1200 nm. The TGA experiments were carried out on a Perkin Elmer Diamond TG/DTG analyzer instrument with a heating rate of 10 °C/min in nitrogen atmosphere.

2. Crystallography

The single crystal X-ray diffraction studies were carried out using a Bruker AXS Kappa Apex 2CCD diffractometer, with graphite monochromated Mo K α ($\lambda = 0.71073 \text{ \AA}$). The unit cell dimensions and intensity data were recorded at 296 K. The program SAINT/XPREP

was used for data reduction and APEX2/SAINT for cell refinement⁶. The structure was solved using SIR92⁷ and refinement was carried out by full-matrix least squares on F^2 using SHELXL-97⁸. All non-hydrogen atoms were refined with anisotropic thermal parameters. All CH_2 hydrogen atoms were geometrically fixed and refined using a riding model. Hydrogen atoms of all the water

molecules were located. Molecular graphics employed were DIAMOND Version 3.1 f⁹.

Results and Discussion

The single crystals of TAFZ appeared at the gel solution interface after 17 days the optimum conditions to obtain best quality crystals and are presented in table 1 and the photograph of as grown crystal was presented in figure 1

Table 1. Optimum conditions for the growth of TAFZ single crystals

Parameters	Optimum Conditions
Density of sodium metasilicate solution	1.03 gcm^{-3}
pH	5
Temperature	Room temperature
Concentration of fumaric acid	1 M
Concentration of zinc sulphate solution	1 M
Gel setting done	10 days
Period of growth	17 days

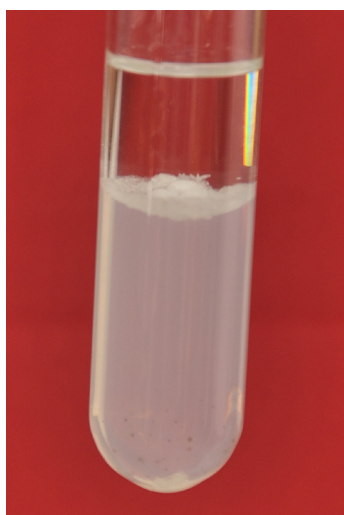


Figure 1. Photograph of grown crystals of TAFZ in boiling tube

The result of elemental analysis was presented in table 2 shows which is in good agreement with the theoretical values of single crystal of TAFZ, $[\text{Zn}(\text{C}_4\text{H}_2\text{O}_4)(\text{H}_2\text{O})_4]$. The presence of coordinated water molecules are confirmed from the crystal structure of the compound.

Table 2. Percentage compositions of C and H of TAFZ

Element	Experiment (%)	Theoretical (%)
C	19.0	19.1
H	3.7	3.9

The UV-visible spectrum of the complex is presented in figure 8. There is a small peak at 243 nm corresponding to intra ligand charge transfer. The lower cut off wavelength is observed at 238 nm and the compound is transparent

to all the visible radiations in accordance with the d^{10} configuration of $\text{Zn}(\text{II})$ ion¹¹.

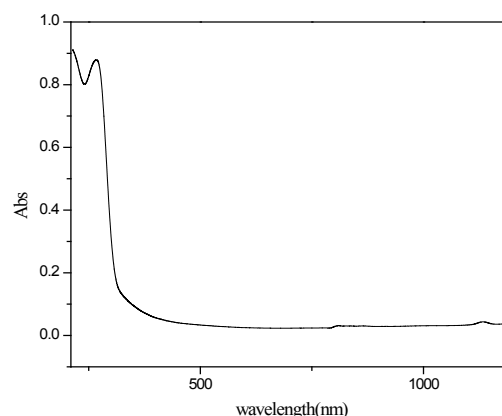


Figure 8. Absorption spectrum of TAFZ crystal

The FT-IR spectrum of fumaric acid exhibits a strong band at 1674 cm^{-1} due to $\nu(\text{C}=\text{O})$ vibration of COOH group which is absent in TAFZ shows the ligand coordination around the metal ions in the deprotonated fumarate form. The asymmetric stretching vibrations are present in 1574 cm^{-1} and symmetric stretching vibrations are observed in 1398 cm^{-1} supporting the monodentate coordination of fumarate¹². This is confirmed from the single crystal X-ray diffraction studies. There is a broad band in the wave number range $3100\text{-}3500 \text{ cm}^{-1}$ indicating O-H stretching frequency of water molecules. The weak band observed at 2326 cm^{-1} corresponds to CH_2 symmetric stretching vibrations. The bands at 1204 cm^{-1} and 978 cm^{-1} are due to asymmetric and symmetric stretching vibrations of C-C bond. The band at 695 cm^{-1} is due to COO^- bending vibrations. The IR spectrum of TAFZ is shown in figure 9.

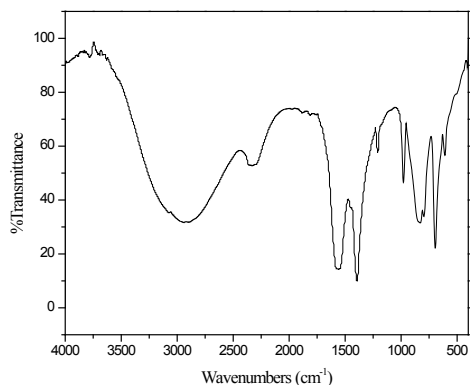


Figure 9. FT-IR spectrum of TAFZ crystal

1. Powder X-ray diffraction studies

The powder X-ray diffractogram of TAFZ crystal is shown in figure 2, the simulated data for the single crystal using Mercury software¹⁰ was also presented. The sharp peak at 31.0857 Å confirms the crystallinity of the compound. The d-values of the Bragg peaks were checked using JCPDS software and no matches were found which shows that powder XRD pattern of the crystal is not reported in the literature. The similarity of the experimental powder crystal data with the single crystal simulated data shows the bulk purity of the crystal. The sharp peaks matched well which confirms that the crystal structure obtained from single crystal XRD is representative of the entire sample.

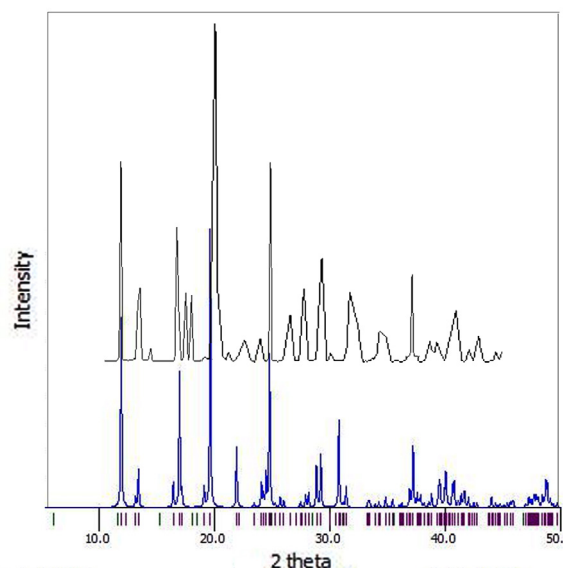


Figure 2. Simulated and experimental powder X-ray patterns of TAFZ crystal

2. Crystal structure of TAFZ

The crystal data and structure refinement parameters are presented in table 3 and selected bond lengths and bond angles are summarized in table 4. The structure of TAFZ consists of a one dimensional metal organic framework system linking zinc– fumarate–zinc fragments. The compound crystallizes in monoclinic with space group $P2_1/c$. The asymmetric unit of TAFZ crystal with atom numbering scheme is given in figure 3.

Table 3. Crystal data and structure refinement parameters for TAFZ

Empirical formula	$C_4 H_{10} O_8 Zn$
Formula weight	251.49
Temperature	296(2) K
Wavelength	0.71073 Å
Crystal system, space group	Monoclinic, $P2_1/c$
Unit cell dimensions	$a = 7.5007(3)$ Å, $\alpha = 90^\circ$ $b = 14.3505(6)$ Å, $\beta = 99.662(2)^\circ$ $c = 7.6901(3)$ Å, $\gamma = 90^\circ$
Volume	816.01(6) Å ³
Z, Calculated density	4, 2.047 Mg/m ³
Absorption coefficient	3.026 mm ⁻¹
F(000)	512
Crystal size	0.35 x 0.30 x 0.25 mm
Theta range for data collection	2.75 to 28.33°
Limiting indices	$-9 \leq h \leq 9$, $-19 \leq k \leq 19$, $-10 \leq l \leq 10$
Reflections collected / unique	14566 / 2019 [$R(\text{int}) = 0.0364$]
Completeness to theta = 24.99	99.1 %
Absorption correction	Semi-empirical from equivalents
Max. and min. transmission	0.5184 and 0.4173
Refinement method	Full-matrix least-squares on F^2
Data / restraints / parameters	2019 / 0 / 159
Goodness-of-fit on F^2	1.097
Final R indices [$I > 2\sigma(I)$]	$R_1 = 0.0187$, $wR_2 = 0.0493$
R indices (all data)	$R_1 = 0.0201$, $wR_2 = 0.0500$
Extinction coefficient	0.0195(11)
Largest diff. peak and hole	0.584 and -0.513 e. Å ⁻³

$$R_1 = [\sum w||F_o| - |F_c||] / \sum |F_o|, wR_2 = [\sum w(F_o^2 - |F_c|^2)^2 / \sum w(F_o^2)]^{1/2}$$

Table 4. Selected bond lengths and bond angles of TAFZ

bond lengths (Å)		Bond angles (°)	
Zn(1)-O(4)	2.0627(11)	O(4)-Zn(1)-O(1)	92.89(5)
Zn(1)-O(1)	2.0886(10)	O(4)-Zn(1)-O(8)#1	91.73(4)
Zn(1)-O(8)#1	2.0902(9)	O(1)-Zn(1)-O(8)#1	173.88(4)
Zn(1)-O(5)	2.1033(10)	O(4)-Zn(1)-O(5)	90.44(4)
Zn(1)-O(3)	2.1076(10)	O(1)-Zn(1)-O(5)	84.25(4)
Zn(1)-O(6)	2.1340(11)	O(8)#1-Zn(1)-O(5)	91.71(4)
O(2)-C(1)	1.2423(17)	O(4)-Zn(1)-O(3)	177.88(4)
O(1)-C(1)	1.2726(16)	O(1)-Zn(1)-O(3)	87.88(4)
O(7)-C(4)	1.2468(16)	O(8)#1-Zn(1)-O(3)	87.63(4)
O(8)-C(4)	1.2749(16)	O(5)-Zn(1)-O(3)	91.59(4)
C(3)-C(2)	1.3217(19)	O(4)-Zn(1)-O(6)	91.94(4)
C(3)-C(4)	1.4924(18)	O(1)-Zn(1)-O(6)	93.99(4)
C(1)-C(2)	1.4963(18)	O(8)#1-Zn(1)-O(6)	89.85(4)
		O(5)-Zn(1)-O(6)	177.11(4)
		O(3)-Zn(1)-O(6)	86.04(4)
		C(1)-O(1)-Zn(1)	127.85(9)
		C(4)-O(8)-Zn(1)#2	128.07(9)
		O(2)-C(1)-O(1)	124.70(12)
		O(2)-C(1)-C(2)	120.14(12)
		O(1)-C(1)-C(2)	115.14(12)
		O(7)-C(4)-O(8)	123.87(12)
		O(7)-C(4)-C(3)	119.34(12)
		O(8)-C(4)-C(3)	116.77(12)

Symmetry transformations used to generate equivalent atoms:

#1 $x-1, y, z-1$ #2 $x+1, y, z+1$

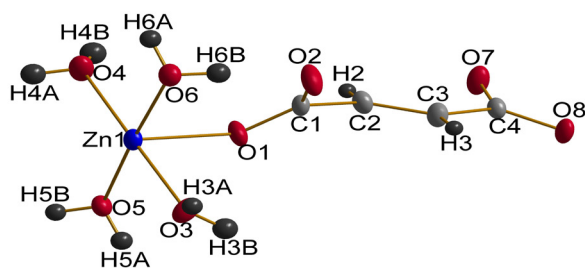


Figure 3. Asymmetric unit of TAFZ with atom numbering scheme

The metal centre Zn(II) is six coordinated with respect to oxygen atoms of which two are from fumarate moieties and four are from coordinated water molecules with Zn—O distances in the range 1.2423 (17)–2.1340 (10) Å. Of the four coordinated water molecules, two are arranged above and the other two below the metal centre. Among these O4 is arranged perpendicular to O3 and O5 is arranged perpendicular to O6. One fumarate moiety is present in the asymmetric unit with the carboxylate groups adopting a monodentate coordination mode. The coordination geometry can be best explained as distorted octahedral geometry. The structure as a whole can be viewed as the fumarate ligands connecting the metal centers, building a one dimensional chain. Packing diagram of the crystal along a, b and c axis are presented in figure 4, 5 and 6 respectively.

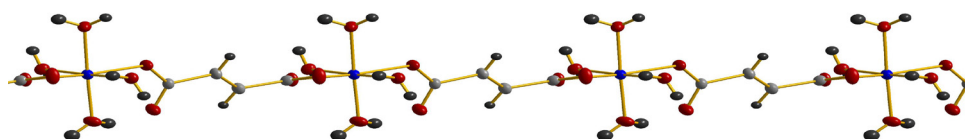


Figure 4. Perspective view of the 1D chain of TAFZ along a axis

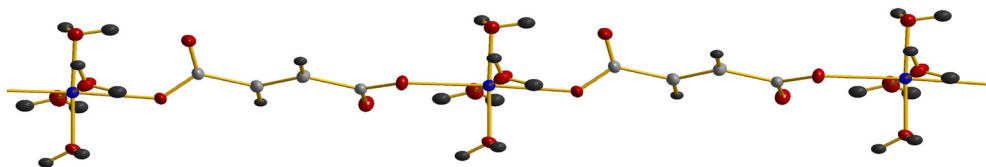


Figure 5. Perspective view of the 1D chain of TAFZ along b axis

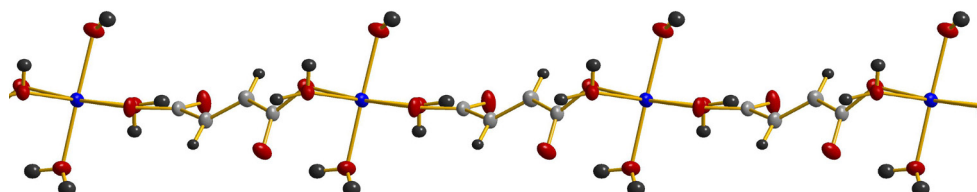


Figure 6. Perspective view of the 1D chain of TAFZ along c axis

The compound consists of four coordinated water molecules and these undergo hydrogen bonding across the crystal. One of the hydrogen atoms (H3B, H6B in figure) of each of the coordinated water molecules are hydrogen bonded to oxygen atom of the fumarate moiety (O1, O8) and the oxygen atoms of the coordinated water

molecules (O3, O4 in figure) are hydrogen bonded to hydrogen atoms (H3A, H5A, H6A in figure) of the other coordinated water molecules. The pattern of hydrogen bond is shown in figure 7 and the parameters of hydrogen bonding are summarized in table 5.

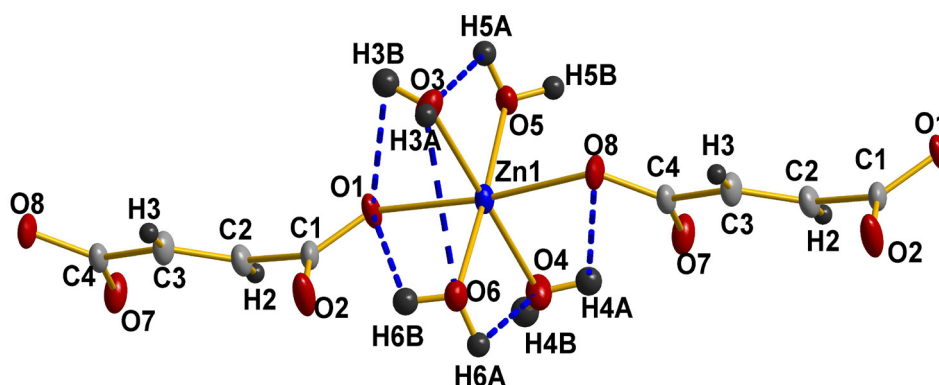


Figure 7. Hydrogen bonding in TAFZ

Table 5. Geometries of the H-bonds in TAFZ

D-H	d(D-H) (Å)	D(H···A) (Å)	d(D-A) (Å)	∠(D-H···A) (°)
O3-H3A	0.787	2.043	2.824	172.18
O3-H3B	0.753	2.105	2.852	171.68
O6-H6A	0.810	1.903	2.701	168.45
O6-H6B	0.780	1.943	2.676	156.66
O5-H5B	0.760	1.945	2.705	178.37
O5-H5A	0.765	1.976	2.717	162.93
O4-H4A	0.792	1.910	2.639	152.60
O4-H4B	0.739	2.177	2.913	173.75

O1 [x, -y+1/2, z-1/2], O6 [x, -y+1/2, z+1/2], O7 [-x+1, -y, -z+1], O8 [x-1, -y+1/2, z-1/2], O2 [x-1, y, z], O7 [x-1, y, z-1], O5 [-x, -y, -z+1]

With these hydrogen bonds the molecule constructs the supramolecular framework with the presence of open channels along c axis (Figure 8).

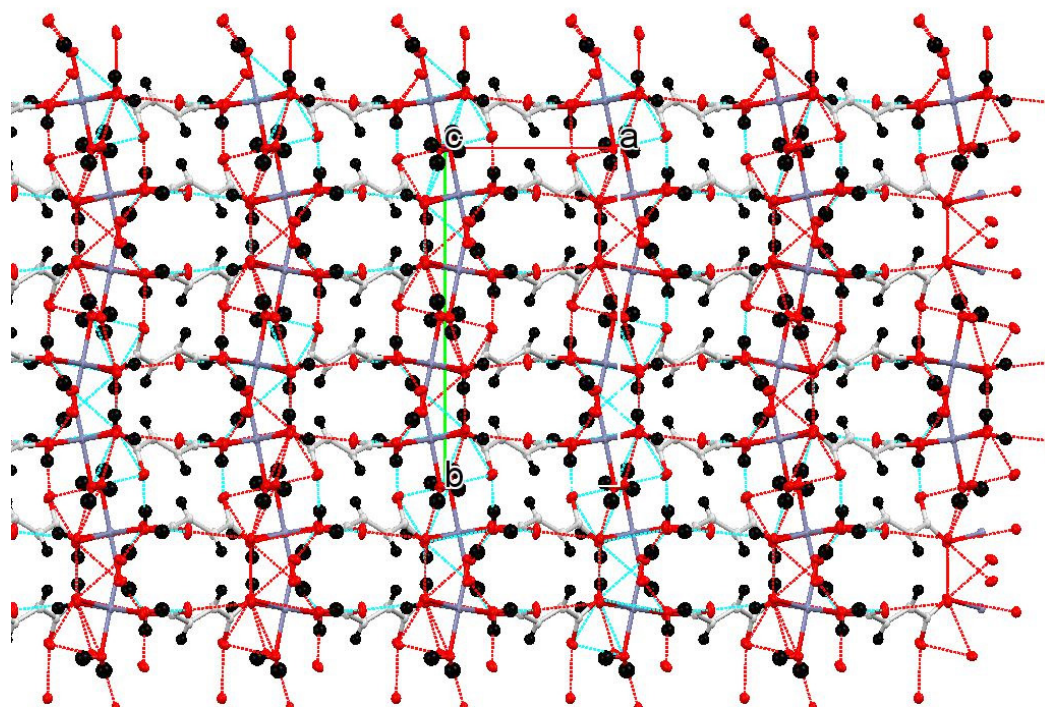


Figure 8. Supramolecular framework of TAFZ through hydrogen bonds

3. Thermal studies

The results obtained from TGA are shown in figure 9. The dissociation of the crystal takes place in three steps. The first stage of decomposition is completed at 107 °C with an observed weight loss 5.1% (4.0% calc.) which corresponds to the removal of one of the coordinated water molecules. The loosely bound water molecule is eliminated first and the rest of the water molecules liberates along with the next decomposition. The second stage of decomposition ends at 459 °C with an observed weight loss of 46.1% (46.3% calc.) which corresponds to the decomposition of zincfumaratetrihydrate to zinc carbonate. The final product of the decomposition may be ZnO.

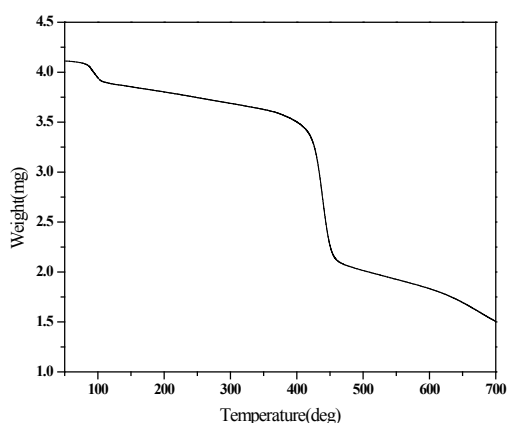


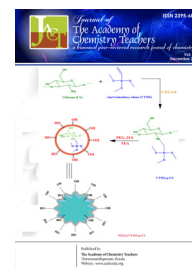
Figure 9. TGA of TAFZ

4. Conclusion

This chapter describes the growth and characterization of tetraaquafumaratozinc(II) grown by single gel diffusion technique at room temperature. The crystals obtained were colourless and transparent. The grown crystals were characterized by elemental analysis and UV-visible spectral studies. The crystallinity of the grown crystals was confirmed by powder X-ray diffraction studies. The single crystal data was simulated using the software Mercury and was compared with the powder XRD data and the bulk purity of the crystal was confirmed. Monodentate coordination of the carboxylate part of the fumarate moiety to the zinc ion is identified by FT-IR spectral studies. Crystal structure of the compound was elucidated by single crystal X-ray diffraction studies which show that the compound is having a 1D chain structure with hydrogen bonding forming a supramolecular framework.

References

1. Lehn J M, Chem Soc Rev, 36, **2007**, 151-160.
2. Nicola C D, Forlin E, Garau F, Lanza A, Natile M M, Nestola F, Pandolfo L & Pettinari C, J Organomet Chem, 714, 2012, 74-80.
3. Zhang, K L, Liang W, Chang Y, Yuan L M, Ng S W, Polyhedron, 28(4), **2009**, 647-652.
4. Gupta M P, Sahu R D, Maulik P R, Z. Crystallogr, 163, **1983**, 151-154.
5. Want B, Ahmad F, Kotru P N, Cryst. Res. Technol, 41(12), **2006**, 1167-1173.
6. Bruker, APEX2, SAINT, XPREP, Bruker AXS Inc. Madison, Wisconsin, USA, **2004**.
7. Altornare A, Cascarano G, Giacovazzo C, Guagliardi A, J. Appl. Cryst, 26(3), **1993**, 343-350.
8. Sheldrick G M, 'SHELXS97. Program for the Solution of Crystal Structures', University of Gottingen, Germany, **1997**.
9. Brandenburg K, Diamond Version 3.1f, Crystal Impact GbR, Bonn, Germany, **2008**.
10. Bruno I J, Cole J C, Edgington P R, Kessler M, Macrae C F, Mc Cabe P, Pearson, J, Taylor R, Acta. Cryst, 58B(3-1), **2002**, 389-397.
11. Sivasankar B N, Govindarajan S, Taylor and Francis, 24(9), **1994**, 1573-1582.
12. Nakamoto K, 'Infrared and Raman Spectra of Inorganic and Coordination Compounds'. Part B, 5th Edn., Wiley-Interscience, New York, **1997**.



A Glimpse to Thermal Decomposition Kinetics in Solid State

Jeena John, Sudha Devi R, Balachandran S*

Department of Chemistry, Mahatma Gandhi College, Kesavadasapuram - Thiruvananthapuram, Kerala, India-695 004

*Author for correspondence:

E-mail: sbcnair@gmail.com

Abstract

Thermogravimetric analysis (TG) or thermal gravimetric analysis (TGA) is commonly used to determine the characteristic decomposition patterns, materials characterization through analysis, determination of organic or inorganic content in a sample and studies of degradation mechanisms and reaction kinetics by analyzing the mass deviation on heating. The kinetic principles of thermal process can be easily derived by Isothermal process; however non isothermal procedures are usually adopted due to less time consumption and easy instrumental techniques. Many reaction models were proposed depending on the nature of reaction and the present review is only a glimpse towards the topic concerned.

Introduction

Thermal analysis deals with measuring changes in physical properties of materials on heating or cooling as a function of time and it is extremely useful for the characterization of solids. Thermal analysis aimed to qualitatively identify thermally induced transformation and determine the transformation temperature. The beginning of thermal analysis is by the works of Roberts-Austen^{1,2} who recorded the temperature difference between a sample and reference material as a function of time and temperature, the first differential thermal analysis (DTA). The first thermogravimetry (TG), instrument, Honda's thermobalance³, was introduced in 1915. Ten years after the development of Honda's thermobalance, Kujirai and Akahira⁴ evaluated the effect of temperature on the deterioration of six different fibrous insulating materials, and developed an empirical expression of the Arrhenius-type equation for the reactions.

$$\log t = \frac{Q}{T} - F(w) \dots \dots \dots (1)$$

where Q and w are the process constant and mass-loss fraction, respectively.

In the mid-20th century, TG and DTA became common and commercially available. Subsequently, instrument improvement based on experiments and theoretical analysis enabled to quantitatively determine the changes in the physical properties, such as enthalpy change and mass-change. Presently thermal analysis is a powerful tool for recording the kinetic rate data of thermally induced chemical and/or physical processes. Many researchers have tried to apply thermal analysis to the kinetic characterization of thermally induced processes in various materials^{5,6}.

Reaction kinetics in the solid-state can be studied not only by thermogravimetry, but also using other analytical

methods such as differential scanning calorimetry (DSC)^{7,8}, powder X-ray diffraction (PXRD)⁹, and nuclear magnetic resonance (NMR)^{10,11}.

For any thermally stimulated processes, thermal analysis and its rate can be parameterized in terms of three major variables: the temperature, T; the extent of conversion, α and the pressure, P.

$$\frac{d\alpha}{dt} = k(T)f(\alpha)h(P) \dots \dots \dots (2)$$

The pressure dependence, h(P) is ignored in most of kinetic computational methods even though the pressure may have a profound effect on the kinetics of processes, whose reactants and/or products are gases. The majority of kinetic methods used consider the rate to be a function of only two variables, T and α

$$\frac{d\alpha}{dt} = k(T)f(\alpha) \dots \dots \dots (3)$$

Where f(α) is the reaction model, k_(T) is the temperature dependant rate constant. α is the extend of reaction and for isothermal thermogravimetric measurement, it is defined as

$$\alpha = \frac{m_0 - m_t}{m_0 - m_\infty} \dots \dots \dots (4)$$

where, m_0 is initial weight, m_t is weight at time t, and m_∞ is final weight. Non-isothermally α at any temperature is

$$\alpha = \frac{m_0 - m_T}{m_0 - m_\infty} \dots \dots \dots (5)$$

Where m_T is the sample weight at temperature, T.

The dependence of the process rate on temperature is represented by the rate constant, k(T), and the dependence on the extent of conversion by the reaction model, f(α). For a process that accompanied by mass loss,

the extent of conversion is evaluated as a fraction of the total mass loss in the process represented by equation 3.

If a process is accompanied by release or absorption of heat, the extent of conversion is evaluated as a fraction of the total heat released or absorbed in the process. The rate constant, k , usually has an Arrhenius temperature dependence¹²⁻¹³

$$K(T) = Ae^{-Ea/RT} \dots \dots \dots (6)$$

Replacing $k(T)$ in equation 3 with the Arrhenius equation, gives equation 7

$$\frac{d\alpha}{dt} = Ae^{-Ea/RT} f(\alpha) \dots \dots \dots (7)$$

Where Ea is the activation energy, A is the pre-exponential factor and R is the universal gas constant¹²⁻¹³.

Methods to study solid state kinetics

The International Confederation for Thermal Analysis and Calorimetry (ICTAC) Kinetics Committee provide expert advice on the efficient use of thermal methods and recommended the use multiple heating rate programs for the determination of reliable kinetic parameters, while methods that use a single heating rate program should be avoided. If a single heating rate program is used errors will occur due to the deviation of sample temperature by the limited thermal conductivity or the thermal effect of the process that may lead to self-heating/cooling.

The use of small sample mass can reduce these effects; however runs on samples of two markedly different masses (e.g., 10 and 5mg) and making sure that the obtained data give rise to the kinetic curves that can be superposed is recommended. Otherwise, the sample mass needs to be decreased until the superposition are accomplished. The temperature program can be isothermal, $T = \text{constant}$, or nonisothermal, $T = T(t)$.

Kinetic analysis can have either a practical or theoretical purpose. The practical purpose is the prediction of process rates and material lifetimes which is reliable only when sound kinetic analysis methods are used. The theoretical purpose of kinetic analysis is interpretation of experimentally determined kinetic triplets the reaction model (α), A and Ea which can be obtained from isothermal kinetic data by applying the a rate law (equation 6). Each of the components of a kinetic triplet is associated with some fundamental theoretical concept. Ea is associated with the energy barrier, A with the frequency of vibrations of the activated complex, and $f(\alpha)$ or $g(\alpha)$ with the reaction mechanism.

The solid state reaction models allows the determination of most suitable $f(\alpha)$ or $g(\alpha)$ value associated with the thermal degradation of solids. Experimental and computational methods are widely used for these studies. In experimental method the suitable functions can be determined in two ways: isothermally, with temperature maintained constant over time, or non-isothermally, with the variation in both temperature and time dependent on the heating rate (β). Some methods are based on a single β -model fitting, whereas others are multiple heating rate model-free methods, also known as isoconversional

methods. The isoconversional methods are considered to be the best approach for truly determining the apparent Ea ¹²⁻¹³.

Isothermal and Non-isothermal measurements

In isothermal method sample is maintained at several constant temperatures and as a result at each temperature a set of α -time points is produced. In non-isothermal method the temperature of the solid is changed under controlled and constant heating rate, $\beta = dT/dt$. In such cases the degree of conversion α can be calculated as a function of temperature which depends on time of heating¹²⁻¹³. Therefore the rate of reaction can be written as

$$\frac{d\alpha}{dt} = \frac{d\alpha}{dT} \frac{dT}{dt} = \beta \frac{d\alpha}{dT} \dots \dots \dots (8)$$

where, da/dT is the non-isothermal reaction rate, da/dt is the isothermal reaction rate, and dT/dt is the heating rate (β).

The rate equation described by Eq. 7 can be converted to a non-isothermal rate expression by relating the rate of reaction as a function of temperature at constant heating rate β . Then equation 7 will change to 9, where β is the heating rate.

$$\frac{d\alpha}{dT} = \frac{A}{\beta} e^{(-Ea/RT)} f(\alpha) \dots \dots \dots (9)$$

Separating variables and integrating equations (9) from initial temperature T_0 to a peak temperature T_m gives the integral forms of the non-isothermal rate law as

$$\int_0^\infty \frac{d\alpha}{f(\alpha)} = \frac{A}{\beta} \int_{T_0}^{T_p} e^{-Ea/RT} dT \dots \dots \dots (10)$$

where $\int_0^\infty \frac{d\alpha}{f(\alpha)} = g(\alpha)$, the integral reaction model, then equation 10 will change to

$$g(\alpha) = \frac{A}{\beta} \int_0^T e^{(-Ea/RT)} dT \dots \dots \dots (11)$$

The lower boundary of the integral form is eliminated by assuming T_0 as the temperature where the decomposition rate cannot be measured. By substituting $-Ea/RT = X$, equation 11 can be rearranged as follows

$$g(\alpha) = \frac{AEa}{\beta R} \left(\frac{\exp^X}{X} + \int_0^\infty \frac{\exp^X}{X} dX \right) = \left(\frac{AEa}{\beta R} \right)^{p(X)} \dots (12)$$

The exponential integral ($P(x)$) has no analytical solution but has many approximations¹⁴⁻¹⁷. In order to solve $p(X)$, this function want to be convert to an approximate form that can be integrated or want to approximate by a series expansion. Commonly used approximation methods are Doyle approximation and Senum- Yang approximation. The two series widely used for approximating the temperature integral are asymptotic series expansion and Schlomilch series expansion¹².

There are different methods to study the kinetics of non-isothermal processes. These include statistical methods¹⁸⁻²², predictions of activated complex theory for the value of the pre-exponential factor²³, methods based

on the fact that, for different reaction models, the extent of reaction at maximum reaction rate a max falls into a narrow specific range²⁴.

Model fitting isoconversional method

Commonly Kinetic parameters can be obtained from non-isothermal rate laws by both model fitting and isoconversional (model free) methods. Force-fitting experimental data to different model function $f(\alpha)$ is denoted as model-fitting methods, after the $f(\alpha)$ model has been selected from the best linear fit for a series of temperature, $k(T)$ is evaluated²⁵.

Finding most suitable $f(\alpha)$ or solid state reaction model

The thermal and kinetic aspects of solid state composition reactions are complex²⁶⁻³⁰ since it depends on the factors such as rate of nuclei formation, interface advance, diffusion and geometrical shape of solid particles. The involvement of these factors in solid state decomposition reaction results in the development of several decomposition models. The function $f(\alpha)$ in Eq. (7) can take many forms depending on the type of reaction that occurs. A summary of these reaction models were listed in table 1.

The solid state reaction models are generally classified by mechanistic assumption or by the shape of isothermal

α versus time or $d\alpha/dt$ versus α plots. By mechanistic assumption, models are classified as nucleation, diffusion, geometrical contraction and reaction order models. Both A and P models comes under the category of nucleation model which accounts for both nucleation and nuclei growth rate. In nucleation model the rate limiting step is the formation and growth of nuclei. In this model rate of nuclei formation and growth is different. In geometrical contraction an instantaneous nucleation occurs in the surface of solid and progress of this reaction is the rate limiting step. In diffusion model the rate limiting step is diffusion of reactants into reaction sites. In reaction order described are similar to the order of the reaction used in homogeneous kinetics¹²⁻¹³.

Based on the shape of α versus time plots, models can be categorized as linear, acceleratory, deceleratory or sigmoidal model. In acceleratory model reaction rate increases as reaction progresses where in deceleratory model the reaction rate decreases with increase in reaction rate. In linear model the reaction rate will remains constant and in sigmoidal model a bell shaped relation will be obtained¹²⁻¹³. The solid state reaction models based on all these classifications are summarized in table 1.

No	Symbol	Rate determining mechanism	$f(\alpha)$	$g(\alpha)$
I	Chemical processes			
1	$F_{1/3}$	Chemical reaction	$3/2(1-\alpha)^{1/3}$	$1-(1-\alpha)^{2/3}$
2	$F_{3/4}$	Chemical reaction	$4(1-\alpha)^{3/4}$	$1-(1-\alpha)^{1/4}$
3	$F_{3/2}$	Chemical reaction	$2(1-\alpha)^{3/2}$	$(1-\alpha)^{-1/2}-1$
4	F_2	Chemical reaction	$(1-\alpha)^2$	$(1-\alpha)^{-1}-1$
5	F_3	Chemical reaction	$1/2(1-\alpha)^3$	$(1-\alpha)^{-2}-1$
6	F_4	Chemical reaction	$1/3(1-\alpha)^4$	$(1-\alpha)^{-3}-1$
7	G_1	Chemical reaction	$1/2(1-\alpha)$	$1-(1-\alpha)^2$
8	G_2	Chemical reaction	$1/3(1-\alpha)^2$	$1-(1-\alpha)^3$
9	G_3	Chemical reaction	$1/4(1-\alpha)^3$	$1-(1-\alpha)^4$
II	Acceleratory rate equations			
10	$P_{3/2}$	Nucleation	$(2/3)\alpha^{-1/2}$	$\alpha^{3/2}$
11	$P_{1/2}$	Nucleation	$2\alpha^{1/2}$	$\alpha^{1/2}$
12	$P_{1/3}$	Nucleation	$3\alpha^{2/3}$	$\alpha^{1/3}$
13	$P_{1/4}$	Nucleation	$4\alpha^{3/4}$	$\alpha^{1/4}$
14	E_1	Nucleation	$\ln\alpha$	α
III	Sigmoid rate equations			
15	$A_{1,2}F_1$	Assumed random nucleation and its subsequent growth	$1-\alpha$	$[-\ln(1-\alpha)]$
16	$A_{3/2}$	Assumed random nucleation and its subsequent growth	$3/2(1-\alpha)[- \ln(1-\alpha)]^{1/3}$	$[-\ln(1-\alpha)]^{2/3}$
17	A_2	Assumed random nucleation and its subsequent growth	$2(1-\alpha)[- \ln(1-\alpha)]^{1/2}$	$[-\ln(1-\alpha)]^{1/2}$
18	A_3	Assumed random nucleation and its subsequent growth	$3(1-\alpha)[- \ln(1-\alpha)]^{2/3}$	$[-\ln(1-\alpha)]^{1/3}$
19	A_4	Assumed random nucleation and its subsequent growth	$4(1-\alpha)[- \ln(1-\alpha)]^{3/4}$	$[-\ln(1-\alpha)]^{1/4}$
20	G_4	Assumed random nucleation and its subsequent growth	$1/2(1-\alpha)[- \ln(1-\alpha)]^{-1}$	$[-\ln(1-\alpha)]^2$
21	G_5	Assumed random nucleation and its subsequent growth	$1/3(1-\alpha)[- \ln(1-\alpha)]^{-2}$	$[-\ln(1-\alpha)]^3$

22	G ₆	Assumed random nucleation and its subsequent growth	1/4(1-α)[-ln(1-α)] ³	[-ln(1-α)] ⁴
23	A ₁₁	Branching nuclei	α/(1-α)	ln α/(1-α)
IVa Deceleratory rate equations based on phase boundary reaction				
24	R ₁₂ , F ₀₂ , P ₁	Contracting disk	(1-α) ⁰	α
25	R ₂₂ , F _{1/2}	Contracting cylinder	2(1-α) ^{1/2}	1-(1-α) ^{1/2}
26	R ₃₂ , F _{2/3}	Contracting cylinder	3(1-α) ^{2/3}	1-(1-α) ^{1/3}
IVb Deceleratory rate equations based on the diffusion mechanism				
27	D ₁	One-dimensional diffusion	1/2α	α ²
28	G ₇	Two-dimensional diffusion	4{(1-α)[1-(1-α) ^{1/2}]} ^{1/2}	[1-(1-α) ^{1/2}] ^{1/2}
29	D ₂	Two-dimensional diffusion	[-ln(1-α)] ⁻¹	α+(1-α)ln(1-α)
30	D ₃	Three-dimensional diffusion	3/2(1-α) ^{2/3} [1-(1-α) ^{1/3}] ⁻¹	[1-(1-α) ^{1/3}] ²
31	D ₄	Three-dimensional diffusion	3/2[(1-α) ^{-1/3} -1] ⁻¹	1-(2/3)α-(1-α) ^{2/3}
32	D ₅	Three-dimensional diffusion	3/2(1-α) ^{4/3} [(1-α) ^{1/3} -1] ⁻¹	[(1-α) ^{-1/3} -1] ²
33	D ₆	Three-dimensional diffusion	3/2(1+α) ^{2/3} [(1+α) ^{1/3} -1] ⁻¹	[(1+α) ^{1/3} -1] ²
34	D ₇	Three-dimensional diffusion	3/2[(1+α) ^{-1/3} -1] ⁻¹	1+(2/3)α-(1+α) ^{2/3}
35	D ₈	Three-dimensional diffusion	3/2(1+α) ^{4/3} [(1+α) ^{-1/3} -1] ⁻¹	[(1+α) ^{-1/3} -1] ²
36	G ₈	Three-dimensional diffusion	6(1-α) ^{2/3} [1-(1-α) ^{1/3}] ^{1/2}	[1-(1-α) ^{1/3}] ^{1/2}

Model-free isoconversional methods allow for estimating the activation energy as function of a without choosing the reaction model, the basic assumption of these methods is that the reaction rate of constant extent of conversion α depends only on the temperature. Hence, constant Ea value can be expected in the case of single stage decomposition. The value of α typically reflects the progress of the overall transformation of a reactant to products. The overall transformation can involve multiple steps and for each steps there can be specific extent of conversion, then the overall transformation can be sum yields of each step. The overall transformation process that involves two parallel reactions can be described by

$$\frac{d\alpha}{dt} = k_1(T)f_1(\alpha_1) + k_2(T)f_2(\alpha_2).....(15)$$

where α₁ and α₂ are the specific extents of conversion respectively associated with the two individual reactions (steps) and their sum yields the overall extent of conversion: α = α₁ + α₂.

The temperature dependence of the rate process can be determined by Arrhenius equation and for a single step reaction the equation 2 can be utilized. The determined kinetic parameters are functions of the individual steps. For multi-step process Ea varies with a due to the variation in the relative contributions of single steps to the overall reaction rate. The activation energy determined will be the activation energy barriers of the individual steps^{14,31}.

Model-fitting approach

There are several non-isothermal model-fitting methods. One of the most popular is the Coats Redfern method (CR method)³², which utilizes the asymptotic series expansion in approximating P(x) equation 14, producing the following equation:

$$\ln \frac{g(\alpha)}{T^2} = \ln \left(\frac{AR}{\beta Ea} \left[1 - \left(\frac{2RT}{\beta Ea} \right) \right] \right) - \frac{Ea}{RT}.....(16)$$

where T is the mean experimental temperature

On simplification of Eq. (16) it becomes

$$\ln \frac{g(\alpha)}{T^2} = \ln \left(\frac{AR}{\beta Ea} \right) - \frac{Ea}{RT}.....(17)$$

where, α is the fraction of decomposition, dα/dt the rate of conversion, β the linear heating rate, A the pre-exponential factor, Ea the apparent activation energy, R gas constant, T the absolute temperature, f(α) and g(α) the differential and integral mechanism functions, respectively.

Achar equation which can be used similar to CR equation is³³

$$\ln \left[\frac{d\alpha/dt}{f(\alpha)} \right] = \ln A - \frac{E}{RT}.....(18)$$

The other method proposed by Clark and Kennedy (CK method) is based on the expression, T = βt + T⁰, where T⁰ is initial temperature. The basic equation is:

$$\frac{\beta g(\alpha)}{T-T^0} = Ae^{(-Ea/RT)}.....(19)$$

Taking the logarithm of both sides of the equation:

$$\ln \frac{\beta g(\alpha)}{T-T^0} = \ln A - \frac{Ea}{RT}.....(20)$$

Plotting the left-hand side of both equations 17, 18 & 20 against 1/T should give straight lines for the reaction models listed inTable 1. From the slope and intercept we can determine Ea and lnA, respectively³⁴.

When the kinetic function model determined was a simple order function model, MKN method³⁵ (Madhusudanan-Krishnan-Ninan) and HM³⁶ (Horowitz-Metzger) method were also applied to process the TG-DTG data to calculate the kinetics parameters and the accurate reaction order.

The MKN equation is

$$\ln \frac{g(\alpha)}{T^{1.9215}} = \ln \left(\frac{AEa}{\beta R} \right) + 3.7721 - 1.9215 \ln E - \frac{0.12039E}{T}.....(21)$$

The HM equation is

$$\ln g(\alpha) = \ln \left(\frac{ART^2}{\beta E} \right) - \frac{E}{RT} + \frac{E\theta}{RT^2} \dots \dots \dots (22)$$

When the values of E and lnA obtained by different methods are approximately equal for a suggested reaction (Table 1) and have good correlation coefficient that will be the mechanism of the thermal decomposition³⁷

It should be remembered that the kinetic triplets are determined by first selecting a rate equation and then fitting it to experimental data. The determined triplets Ea, A and α depends on whether the selected rate equation adequately represent the essential features of the process mechanism. A mere goodness of statistical fit will not represent the issue of the adequateness of a rate equation to a process mechanism since good data fit can be accomplished by using a physically meaningless equation such as that of a polynomial function. Thus meaningful interpretability of the function is essential via a good understanding the process mechanism in TG analysis. For example, a single-step rate equation cannot generally be adequate for a multi-step mechanism. However, it can provide an adequate kinetic representation of a multi-step process that has a single rate-limiting step

Model free methods

The use of isoconversional or model-free methods is suggestive to calculate Ea values however a reaction model is usually needed for a complete kinetic description of any solid-state reaction. The usual practice is determine Ea values by more than one model free methods with statistical authenticity. Use any standard model fitting method like CR method to determine the kinetic triads with different probable mechanism as given in table 1 and the Ea similar to that received for model free method with proper statistical authenticity is selected as the model for the thermal degradation.

The Kissinger–Akahira–Sunose method³⁸⁻³⁹ (KAS method) is based on the Coats–Redfern approximation of P(x) = (exp(-x))/x² which transformed equation 14 to

$$\ln \left(\frac{\beta}{T^2} \right) = \ln \frac{AR}{Ea g(\alpha)} - \frac{Ea}{RT} \dots \dots \dots (23)$$

Where α is the degree of conversion, Ea is the activation energy of the degradation, A is the pre-exponential factor, R is the universal gas constant, β is the heating rate. Ea can be calculated from the slop of the linear plots

of $\ln \beta / T^2$ vs. $1/T$, for each conversion α.

The Ea value can be also be determined by Osawa method⁴⁰ where the proposed equation is

$$\ln \beta = -1.052 \frac{Ea}{RT} + C \dots \dots \dots (24)$$

Another method proposed by Tang (T method) is based on the approximate formula which introduced into equation 14. Taking the logarithms of both sides

$$\ln \left(\frac{\beta}{T^{1.894661}} \right) = \ln \left[\frac{AEa}{Rg(\alpha)} \right] + 3.635041 - 1.894661 \ln Ea - 1.001450 \frac{Ea}{RT} \dots \dots \dots (25)$$

The Flynn-Wall-Ozawa equation⁴¹⁻⁴²

$$\ln \beta = \ln \left(\frac{0.0048 AEa}{Rg(\alpha)} \right) - 1.0516 \frac{Ea}{RT} \dots \dots \dots (26)$$

A plot of the left-hand sides of both equations (23) and (26) versus 1/T give a group of straight lines at each α which give apparent activation energy from the slope for a particular α without considering a selected model.

The Vyazovkin isoconversional method (VYZ method) utilizes an accurate nonlinear Senium-Yang approximation of P(x) of equation 14, which leads to^{34,43}

$$\Omega = \sum_{i=1}^n \sum_{i \neq j}^n \frac{I(Ea, \alpha, T\alpha, i) \beta_j}{I(Ea, \alpha, T\alpha, j) \beta_i} \dots \dots \dots (25)$$

$$I(Ea, \alpha, T\alpha) = \int_0^{T\alpha} e^{(-Ea, \alpha / RT)} dT \dots \dots \dots (26)$$

where n the number of heating rates, I(Ea,α, Tα) the exponential integral (P(x)) that results from heating rate β. The Ea;α can be determined at any particular value of α by finding the value of Ea for which the objective function Ω is minimized. The temperature integral can be evaluated^{44,45} by several approximations such as Gorbachev, Agrawal and Sivasubramanian and Cai for integration of equation 26.

Kissinger method

The Kissinger method is based on the study of the decomposition reaction at maximum rate and at this

point $d^2\alpha/dt^2 = 0$ and thus Eq (7) will change to

$$\ln \left(\frac{\beta_m}{T_m^2} \right) = \ln \left(\frac{AR}{E} f(\alpha) \right) - \frac{E}{RT_m} \dots \dots \dots (27)$$

Where β_m is the value of dT/dt at the point in which maximum rate is reached⁴⁶.

Friedman method

Friedman method considers the logarithm of conversion rate as a function of the reciprocal temperature at different degrees of conversion. The Friedman equation is

$$\ln \beta \frac{d(\alpha)}{dt} = \ln \left(\frac{d\alpha}{dt} \right) = \ln(Af(\alpha)) - \frac{E}{RT} \dots \dots \dots (28)$$

The plot of ln(da/dt) versus 1/T at constant α for a set of β values gives a family of straight lines with slope -Ea/R⁴⁷.

Kinetic parameters can be determined from data obtained from only two different temperature programs, the use of at least 3–5 programs is recommended. For better accuracy Arrhenius parameters a minimum three temperatures or heating rate with at least one experiment with extreme temperatures or heating rates is recommended. The actual range of temperatures and/or heating rates for a specific situation depends on the measurement precision.

A combination of non-isothermal and isothermal experiments is the best way to properly establish kinetic models. A truly good model should simultaneously fit both non-isothermal and isothermal experiments runs with the same kinetic parameters. The kinetic parameters should show good correspondence over a range of temperatures and/or heating rates for credence. The validity of a kinetic model requires a good fit for the measured and calculated reaction profiles, either rates, or extents of conversion, or both. The present authors used different differential and integral methods Coats Redfern, Broido, Horowitz-Metzger, Madhusudanan-Krishnan-Ninan, Freeman-Carroll, Sharp-Wentworth and Achar method by model fitting approach to study the thermal decomposition of Rubrocurcumin a 1:1:1 complex of

curcumin, boric acid and oxalic acid and showed that the decomposition can be best described by Mapel first order reaction model⁴⁸. However the conformation of reaction model requires a model free approach³⁴ or isoconversional method.

Conclusion

This review is made to provide a summary on the basics of solid state reaction kinetics and various experimental methods available to study solid state kinetics. This review includes the most common reaction models used in the study of solid state decomposition reaction. We hope this review will help those who are interested in solid state kinetics.

References

1. Roberts-Austen W. Report 5. Proc Inst Mech Eng, **1899**, 35.
2. Roberts-Austen W, Fifth report to the alloys research committee, Nature, 59, **1899**, 566.
3. Honda K, Sci Rept Tohoku Imp Univ, Ser I, 4, **1915**, 97.
4. Kujirai T & Akahira T, Sci Paper Inst Phys Chem Res, 2, **1925**, 223.
5. Koga N, J Therm Anal Calorim, 113, **2013**, 1527.
6. Koga N, Sestak J & Simon P, Some fundamental and historical aspects of phenomenological kinetics in the solid state studied by thermal analysis. In: Sestak J, Simon P, editors. Thermal analysis of micro, nano- and non-crystalline materials. Berlin: Springer; 2013. p. 1–28.
7. Khawam A & Flanagan D R, J Pharm Sci, 95, **2006**, 472.
8. Vyazovkin S & Dranca I, J Phys Chem B, 109, **2005**, 18637.
9. Kirsch B L, Richman E K, Riley A E, Tolbert S H, J Phys Chem B, 108, **2004**, 12698
10. Jones A R, Winter R, Florian P & Massiot D, J Phys Chem B 109, **2005**, 4324.
11. Bertmer M, Nieuwendaal R C, Barnes A B & Hayes S E, J Phys Chem B, 110, **2006**, 6270.
12. Khawam A & Flanagan D R, J Pharm Sci, 95, **2006**, 472-98.
13. Khawam A & Flanagan D R, J Phys Chem B, 110, **2006**, 17315-28.
14. Khawam A & Flanagan D R, Thermochim Acta 436, **2005**, 101–112.
15. Chen H J & Lai K M, J of Chem Eng of Japan, 37(9), **2004**, 1172–1178.
16. Doyle C D, J Appl Polym Sci, 5, **1961**, 285.
17. Agarwal R K, Sivasubramanian M S, AIChE J, 33, **1987**, 1212–1214.
18. Sun T, Zhao Y, Jin J & Wang D, J Therm Anal, 45, **1995**, 1105–1109.
19. Hu Q P, Cui X G & Yang Z H, J Therm Anal, 48, **1997**, 1379–1384.
20. Carp O & Segal E, Thermochim Acta, 185, **1991**, 111–118.
21. Varhegyi G, Sazabo P, Jakab E & Till F, J Anal Appl Pyrol, 57, **2001**, 203–222.
22. Maciejewski M. J Therm Anal, 38, **1992**, 51–70.
23. Caballero J A & Conesa J A. J Anal Appl Pyrolysis, 73, **2005**, 85–100.
24. Gao X, Chen D & Dollimore D. Thermochim Acta, 223, **1993**, 75–82.
25. Rodante F, Vecchio S & Tomassetti M, J Pharm and Biomed Anal 29, **2002**, 1031–1043.
26. Yang J, Miranda R, & Roy C, Polymer Degradation and Stability, 73(3), **2001**, 455–461.
27. Akbar J & Iqbal M S, Massey S, & Masih R, Carbohydrate Polymers, 90(3), 2012, 1386–1393.
28. Iqbal M S, Massey S, Akbar J, Ashraf C M, & Masih R, Food Chemistry, 140 (1–2), 2013, 178–182.
29. Yao F, Wu Q, Lei Y, Guo W, & Xu Y, Polymer Degradation and Stability, 93(1), **2008**, 90–98.
30. Núñez L, Fraga F, Núñez M R, & Villanueva M, (). Polymer, 41(12), **2000**, 4635–4641
31. Vyazovkin S & Sbirrazzuoli N, Thermochimica Acta 388, **2002**, 289–298.
32. Coats A W & Redfern J P, Nature, 201 (1), **1964**, 67-72.

33. Achar B N, Bridley G W & Sharp J H, Proc Int Clay Conf, 1, **1966**, 67-73.
34. Vyzovkin S & Wight C, Thermochim Acta 340-341, **1999**, 53-68.
35. Madhusudhanan P M, Krishnan K & Ninan K N, Thermochim Acta 97, **1986**, 189-195.
36. Horowitz H H & Metzger G, Anal Chem, 35, **1963**, 1465-1473.
37. Dunjia W, Zhengdong F & Lianying L, Journal of Wuhan University of Technology-Mater Sci Ed, 22(2), **2007**, 240-244.
38. Kissinger H, J Res Natl Bur Stand, 4, **1956**, 217-221.
39. Akahira T & Sunose T. Joint convention of four electrical institutes. Science Technology, 16, **1971**, 22-31.
40. Ozawa T, Thermochim Acta, 203, **1992**, 159-165.
41. Ozawa T, Bull Chem Soc Jpn, 38, **1965**, 1881-1886.
42. Flynn J H & Wall L A, J Polym Sci Part B, Polym Letter, 4, **1966**, 323-328
43. Jankovic B, Adnadevic B & Jovanovic J, Thermochim Acta 452 (2), **2007**, 106-115.
44. Ghoshal A K & Saha B, Thermochim Acta 451, **2006**, 27-33.
45. Maiti A K, Ghoshal A K & Saha B, Thermochim Acta 444, **2006**, 46-52.
46. Kissinger H L, Anal Chem, 29(11), **1957**, 1702-6
47. Friedman H L, J. Polymer Science Part C: Polymer Letter 6, **1965**, 183-95.
48. John J, Devi R S & Balachandran S, Acta Ciencia Indica, Vol XLII C No 2, **2016**, 121-131.

INSTRUCTIONS TO CONTRIBUTORS

Submission of Manuscripts

JACT welcomes reviews on recent topics in all branches of chemistry. Any work in chemistry can be submitted as original research paper. Submission of an article implies that it has not been previously published. A short article of popular interest to the academic and student community is also solicited.

All manuscripts should be submitted electronically as an attached file from the original e-mail address of corresponding author to Email: mdmullassery@gmail.com.

Manuscripts Preparation

The manuscript must be prepared as MS Word in single column with double line spacing. Illustrations should be in Chem Sketch or Chem Draw or as picture in MS Word Version 6 onwards or as JPEG or TIFF files. Abbreviations if any, should be defined the first time they are used. IUPAC units and symbols are recommended.

Manuscripts should be divided into: Title, Authors, Affiliations, Abstract, Keywords (at least five), Introduction, Materials and Methods, Result and Discussion, Conclusion, Acknowledgements, References, Tables, Figures, Schemes, Captions and Graphical Abstract. All authors' full mailing address, phone numbers and E-mail address should be provided. The corresponding author should be identified with an asterisk mark.

Paper Length: The recommended research paper length is 4 printed pages.

Abstracts: Abstracts should be provided a brief account of the importance of the work, the main results and the extracts of conclusion. It should not exceed 100 words and should not contain any references.

Keywords: 4-6 keywords must be included on a separate line below the main abstract.

Text: The text should be in MS Word, Times New Roman font size 12. Simple running matter in double-spaced from with paragraph separation is suggested. The Illustrations, Figures, Tables, Schemes etc can be embedded in the running matter in appropriate place; however they should be attached separately along with the main article in TIFFS or JPEG formats with proper legends. Every page of the manuscripts, including the title page, references, tables, etc. should be numbered.

References: References should be given as shown below.

1. Love J C, Estroff L A, Kriebel J K, Nuzzo R G & Whitesides G M, Chem Rev; 105, 2005, 1103-1169. Authors are encouraged to suggest the names of reviewers.

Statement of Ownership and other particulars about
Journal of the Academy of Chemistry Teachers
a biannual peer-reviewed research journal of chemistry

Form IV (See Rule 8)

- | | |
|---|---|
| 1. Place of Publication | : Thiruvananthapuram |
| 2. Periodicity of Publication | : Biannual |
| 3. Publisher's Name
Nationality & Address | : Dr. Manohar D. Mullassery
(General Secretary, ACT) & Asst. Professor of Chemistry
Fatima Mata National College, Kollam email: mdmullassery@gmail.com |
| 4. Printer's Name, Nationality
& Address | : Dr. Manohar D. Mullassery (General Secretary, ACT) & Asst. Professor of
Chemistry, Fatima Mata National College, Kollam. Mob: 9447110857 |
| 5. Name(s) of the printing
press(es) & Address | : Tandem Reprographics,
Statue, Thiruvananthapuram – 695 001 |
| 6. Editor's Name, Nationality
& Address | : Dr. Reena Ravindran (Vice President, ACT)
Associate Professor of Chemistry, Sree Narayana College
Chempazhanthi, Thiruvananthapuram. Mob: 9349321464 |
| 7. Name and address of the
individual who own the
journal | : Dr. Manohar D. Mullassery (General Secretary, ACT) & Asst. Professor of
Chemistry, Fatima Mata National College, Kollam |

For private circulation only

I **Dr. Manohar D. Mullassery**, Asst. Professor of Chemistry, FMN College, Kollam, do hereby declare that the particular given above are true to the best of my belief.

Sd/-

Dr. Manohar D. Mullassery



The Academy of Chemistry Teachers
Thiruvananthapuram, Kerala
www.actkerala.org

